RESEARCH

Open Access

The Effect of Superplasticizers on Eco-friendly Low-Energy One-Part Alkali-Activated Slag

M. Refaie[1] , Alaa Mohsen[1] , El-Sayed A. R. Nasr[1] and Mohamed Kohail[1*]

Abstract

One-part alkali-activated materials (OP-AAM) have become a promising binder with low carbon and energy requirements associated with superior mechanical and durability characteristics. This study aims to employ commercial superplasticizers (naphthalene-based "Nb-SP" and polycarboxylate-based "PCb-SP"), as well as laboratory-prepared one (phenol–formaldehyde sulfanilate "PFS-SP") in enhancing the properties of OP-AAM. The main problem of superplasticizers (SPs) in the AAM is their hydrolysis in the alkaline activator (NaOH) used in the activation reactions. Therefore, the thermo-chemical treatment process was utilized to mitigate the high activator alkalinity by impeding the NaOH in the aluminosilicate precursor matrix. The OP-AAM was fabricated from thermo-chemical treatment powder (TCT-P) resulting from sintering blast furnace slag (GGBFS) with 10 wt% NaOH at 300 and 500 ℃. The XRD-pattern showed that NaOH was impeded in the GGBFS via sodium aluminum silicate phase formation after sintering at 500 ℃. The results showed that the admixed OP-AAM prepared from TCT-P at 500 ℃ greatly enhanced the workability and mechanical properties. The PFS-SP proved its efficiency in improving the properties of OP-AAM prepared TCT-P at 300 and 500 ℃, referring to its high stability in an alkaline medium. While PCb-SP reinforced the properties of OP-AAM prepared from TCT-P at 500 ℃ only, proving that PCb-SP promotes high capability in TCT-P-500 as well as in Portland cement.

Keywords One-part alkali-activated materials, Superplasticizers, Thermo-chemical treatment, Workability, Setting time, Compressive strength

1 Introduction

In recent years, the huge increase in population growth has encouraged the development of infrastructure and the building of modern urban communities (Maher El-Tair et al., 2021; Mohsen et al., 2022a). As a result, the cement industry was expanded to keep pace with this development, although it is considered one of the most harmful industries to the environment. It consumes a huge amount of raw materials and energy resources as well as emits a high amount of CO_2 (Mayhoub et al., 2021; Mohamed et al., 2023; Ramadan et al., 2022a. Therefore, a suitable alternative to cement must be found to face these obstacles. It was found that the most effective way is to incorporate wastes and industrial by-products into building materials (El-Feky et al., 2022; Essam et al., 2023; Mohsen et al., 2022b).

Alkali-activated materials (AAMs) are promising building materials increasingly used instead of cement due to their relatively positive economic and environmental impact (Davidovits, 1993; Hassan et al., 2019; Juenger et al., 2011; Mohsen et al., 2021). Compared to Portland cement-based concrete, AAM-based concrete is distinguished by some remarkable engineering characteristics,

Refaie *et al. Int J Concr Struct Mater* (2023) 17:48

Page 2 of 22

such as low heat of hydration, great early strength, and superb durability in aggressive mediums. The production of AAMs mainly depends on utilizing industrial wastes or clays rich in active aluminum and silicon oxides, such as fly ash, blast furnace slag, metakaolin, etc. (Khaled et al., 2023; Ramadan et al., 2023a, 2023b; Sayed et al., 2022). A strong alkaline activator solution is required to activate the aluminosilicate precursors, such as NaOH, KOH and Na_2SiO_3 (Zhang et al., 2018). Generally, AAMs can be prepared using two techniques: (i) two-part (TP) or (ii) one-part (OP).

The two-part alkali-activated materials (TP-AAMs) are produced by mixing the aluminosilicate source with the alkaline activator solution. TP-AAMs face many challenges in a wide range of uses, as they are difficult to handle in large amounts due to the alkaline activators' irritating and corrosive effect on the human skin, making them risky to workers during mixing, transportation and placement (Luukkonen et al., 2018; Refaat et al., 2023). Also, despite the high viscosity of TP-AAMs, using superplasticizers to enhance their flowability is not applicable, as most superplasticizers are unstable in a strongly alkaline medium (they are highly dissociated) (Palacios & Puertas, 2004, 2005).

Now a days, there is a big contest to utilize superplasticizers to benefit from their properties in enhancing TP-AAMs-based concrete properties. Table 1 summarizes the previous studies that investigated the impact of different superplasticizers on AAMs' fresh and hardened properties. Regarding TP-AAMs, it is concluded that only naphthalene-based superplasticizers can improve workability and rise compressive strength due to their high stability in a strongly alkaline medium. In contrast, other superplasticizers cannot be employed because they negatively affect either workability, strength, or both. Therefore, it is concluded that most superplasticizers used in cement cannot be used in TP-AAMs binders.

As described above, in terms of listing the problems caused by TP-AAMs) their harmful effect on the human body, and the instability of superplasticizers), there must be a quick and fundamental solution to confront these difficulties. One-part alkali-activated materials

Table 1 Literature summary of the impact of different superplasticizers on the properties of alkali-activated materials

Mixing technique	Aluminosilicate precursor	Alkaline activator		Superplasticizer-based	Effect of superplasticizer on the properties of AAMs		Applicable superplasticizer (recommended from previous studies)	References
		Type	Concentration		Workability	Strength		
Two-part	Steel slag	$NaOH + Na_2SiO_3$ solution	$Na_2O = 4\%$	Vinyl	Not affected	Decreased	None	Puertas et al., (2003)
				Polyacrylate	Not affected	Slightly decreased		
	Steel slag	NaOH solution	$Na_2O = 5\%$	Vinyl	Not affected	Slightly increased	Naphthalene	Palacios and Puertas (2005)
				Polycarboxylate	Not affected	No effect		
				Melamine	Slightly increased	Slightly increased		
				Naphthalene	Increased	Increased		
	Steel slag	NaOH solution	3%	Polycarboxylate	Decreased	Not affected	None	Refaie et al., (2023)
				Naphthalene	Increased	Decreased		
	Fly ash	NaOH solution	8 M	Naphthalene	Increased	Not affected	Naphthalene	Nematollahi and Sanjayan (2014)
		$NaOH + Na_2SiO_3$ solution	$Na_2SiO_3/NaOH = 2.5$	Polycarboxylate	Increased	Decreased	Polycarboxylate	
				Melamine	Decreased	Decreased		
				Naphthalene	Slightly increased	Decreased		
	85% Fly ash + 15% Steel slag	Na_2SiO_3 solution	7%	Polycarboxylate	Slightly decreased	N/A	Naphthalene	Xiong and Guo (2022)
				Naphthalene	Increased	N/A		
Dry-mix one-part	50% steel slag + 50% Fly ash	Na_2SiO_3 powder	12%	Polycarboxylate	Increased	Slightly decreased	Naphthalene or polycarboxylate depending on the water/binder ratio	Alrefaei et al., (2019)
				Melamine	Increased	Slightly decreased		
				Naphthalene	Increased	Slightly increased		
	50% steel slag + 50% Fly ash	$Ca(OH)_2 + Na_2SO_4$ powder	$Ca(OH)_2/Na_2SO_4 = 2.5$	Polycarboxylate	Increased	Increased	Polycarboxylate	Alrefaei et al., (2020)
				Melamine	Increased	Increased		
				Naphthalene	Increased	Increased		

Refaie *et al. Int J Concr Struct Mater* (2023) 17:48

Page 3 of 22

(OP-AAMs) may be a suitable solution for these problems by mitigating the high alkalinity of the alkaline activator. There are two methods for preparing OP-AAMs which are dry-mixing and thermo-chemical treatment techniques.

In dry-mixing OP-AAMs, the solid alkaline activator (NaOH, KOH Ca(OH)$_2$, Li(OH)$_2$, K$_2$CO$_3$, and Na$_2$SiO$_3$) was dry mixed with aluminosilicate precursors, then water was added (Hamid Abed et al., 2022; Hosseini et al., 2021; Tan et al., 2022). The dry-mixing OP-AAMs preparation technique still faces many obstacles (i) it requires a high percentage of alkaline activator, which increases the cost and CO$_2$ emission (Askarian et al., 2018, 2019; Yousefi Oderji et al., 2019); the fabricated composite still suffers from handling (unsafe for the user), poor workability, and low mechanical characteristics resulting from the cracks and dry shrinkage caused by the high heat of hydration (Yousefi Oderji et al., 2019). Concerning the poor fresh and hardened properties of dry-mix OP-AAMs, also, several studies tried to utilize different superplasticizers to enhance their properties, as represented in Table 1. The tabulated data reveal that the previous studies either depended on Na$_2$SiO$_3$, which is environment un-friendly and has a high cost, or Ca(OH)$_2$ + Na$_2$SO$_4$, from which AAMs with low mechanical properties were obtained. This indicates these studies tried to move away from using hydroxides as alkaline activators, which causes dissociation for superplasticizers (NaOH and KOH have low cost and environment-friendly respect to Na$_2$SiO$_3$ as well as give high mechanical properties than Ca(OH)$_2$ + Na$_2$SO$_4$). Accordingly, it is concluded that the highly detrimental effect of the alkaline activator in dry-mixing OP-AAMs has not been solved, which means that the stability issue of the superplasticizers has not been solved.

Recently, several studies recommended using a thermo-chemical treatment technique to limit challenges facing OP-AAMs. In thermo-chemical OP-AAMs, the aluminosilicate precursor was dry mixed with a solid alkaline activator, then sintered at elevated temperature, followed by quenching to increase the amorphousity, and finally mixed with water. The main role of the sintering process is to impede the alkaline activator in the aluminosilicate structure to reduce the alkali intensity of the alkaline activator. This approach was granted by Refaat et al. (2021). They approved the sintering of the mixture from steel slag with 10 wt% NaOH at 500 °C is a suitable

solution to produce a safe, economical and eco-friendly product with adequate fresh and hardened properties for in situ application as the effect of the highly alkaline activator has been eliminated. Therefore, it is predicted that the stability and efficiency of commercial superplasticizers will be enhanced in thermo-chemical OP-AAMs.

According to the literature illustrated above, many research gaps must be recovered: (i) by attempting to reduce the alkaline activator effect without affecting the physico-mechanical properties; (ii) by trying to employ commercial superplasticizers available in the market to solve problems of AAMs and (iii) invented low cost and easily prepared superplasticizers suitable for AAMs applications. Therefore, the new approach of this work is studying the effect of different types of commercial and laboratory-invented superplasticizers on the workability, setting time, compressive strength and phase composition of thermo-chemical treated prepared AAMs.

2 Materials
### 2.1 Ground Granulated Blast Furnace Slag and Alkaline Activator
The main binding material used in this study was ground granulated blast furnace slag (GGBFS) as an industrial by-product from steel production supplied from India. GGBFS' mineralogical oxide composition is tabulated in Table 2; it was investigated by X-ray fluorescence (XRF: Xios, model PW-1400). GGBFS has a specific surface area = 4088 cm^2/g, bulk density = 1.15 ton/m^3 and specific gravity = 2.8. The particle size distribution (PSS NICOMP Nano, model N3000) shows that 99% of GGBFS particles are ≤ 16 µm and the d50 is 4 µm as present in Fig. 1. According to the XRF analysis for GGBFS, the sulfate content described as SO$_3$ in the analyzed sample (0.24 wt%) met the requirements of ASTM C989/C989M-22 (2022) maximum limit (4 wt%). Moreover, according to the activity index, the utilized GGBFS was classified as grade 100, revealing its moderate activity. Also, sodium hydroxide pellets (NaOH, 99% purity) delivered from El-Gomhoria Chemical Company, Cairo, Egypt, were used as an alkali activator.

2.2 Superplasticizers
In this study, three types of superplasticizers (SPs) were used, two of them are commercial superplasticizers and the third is laboratory-prepared superplasticizer. The two commercial SPs are: (i) MasterRheobuild-859

Table 2 Oxides composition of GGBFS (mass, %)

SiO$_2$	Al$_2$O$_3$	Fe$_2$O$_3$	CaO	MgO	MnO	TiO$_2$	SO$_3$	LOI	Total
35.40	17.40	1.40	36.87	6.83	0.35	0.11	0.24	0.5	99.1

| GBSS	
%	Particle size
25	2.3
50	4
75	5.8
80	6.4
90	8.3
99	16
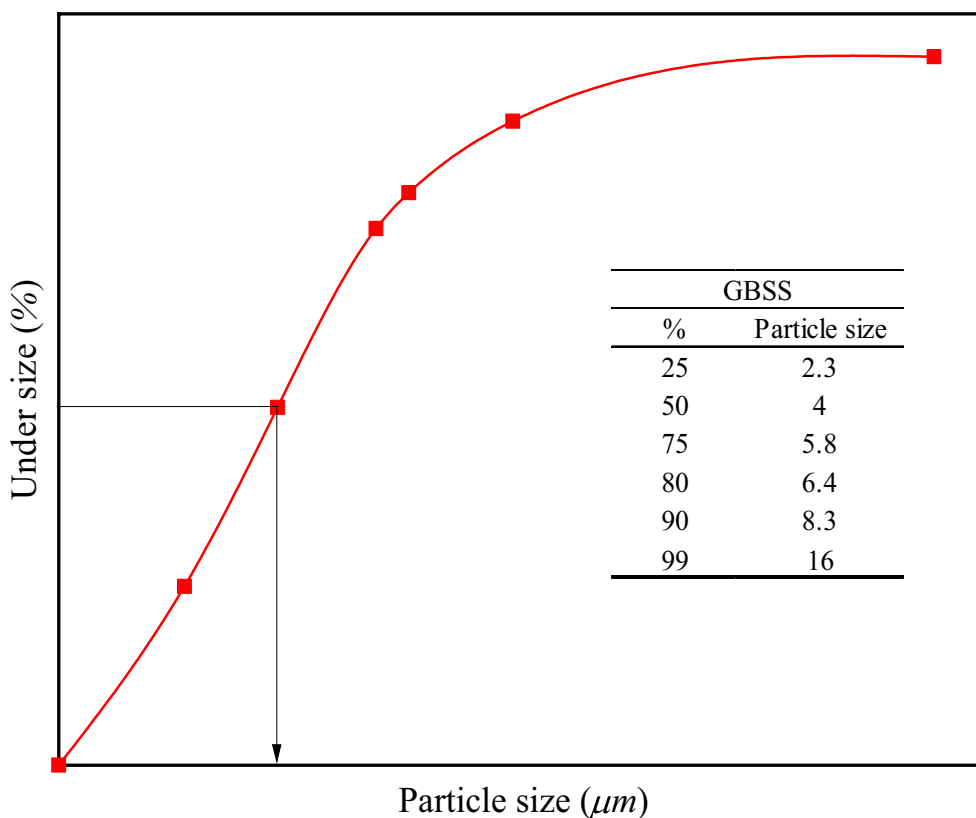
Fig. 1 Particle size distribution of slag

was manufactured by BASF Company, it is a modified naphthalene-based superplasticizer (Nb-SP); and (ii) Viscoflow-10 was synthase by Sika Company (Egypt), it is modified polycarboxylate-based superplasticizer (PCb-SP). The laboratory-prepared SP is a phenol formaldehyde sulfanilate (PFS-SP); a schematic diagram of the preparation technique is plotted in Fig. 2. Table 3 reveals the physical properties of the utilized SPs (color, solid content %, and density). Also, the base chemical compound structures used in preparing these SPs are represented in Fig. 3. Fourier transform infrared (FTIR, Genesis-II spectrometer using KBr) was used to study the main effective function groups of SPs present in wave number ranged between 400 and 4000 cm^{-1} to discuss its effect on the properties of fresh and hardened pastes. Generally, the polymers' (SPs) physical properties depend on the chains' length, which is usually expressed in molecular weight. However, synthetic polymers contain unequal-length chains, referring to polydisperse phenomena. Therefore, the molecular weight is not one value; the polymer presents as a distribution of molecular weights (chain lengths). Consequently, the molecular weight averages of SPs, such as number average molecular weight (Mn) and weight average molecular weight (Mw), as well as polydispersity index (PDI) were measured using gel permeation chromatography (GPC). The Mn is the statistical average molecular weight of the chains in the polymer sample. In contrast to Mn, Mw considers the chains' molecular weight when calculating the molecular weight average. The greater the mass of the chain, the greater the chain's contribution to Mw. PDI refers to polydispersity; if it equals 1, it refers to monodisperse polymer where the lengths of all chains are equal, while if it > 1, it refers to polydisperse polymer where the lengths of all chains are unequal. Mn, Mw and PDI were calculated according to the following equations:

$$\text{Mn} = \frac{\sum N_i M_i}{\sum N_i} \quad \text{Mw} = \frac{\sum N_i M_i^2}{\sum N_i M_i} \quad \text{PDI} = \frac{Mw}{Mn}$$

where Mi is the molecular weight of a chain and Ni is the number of chains of that molecular weight.
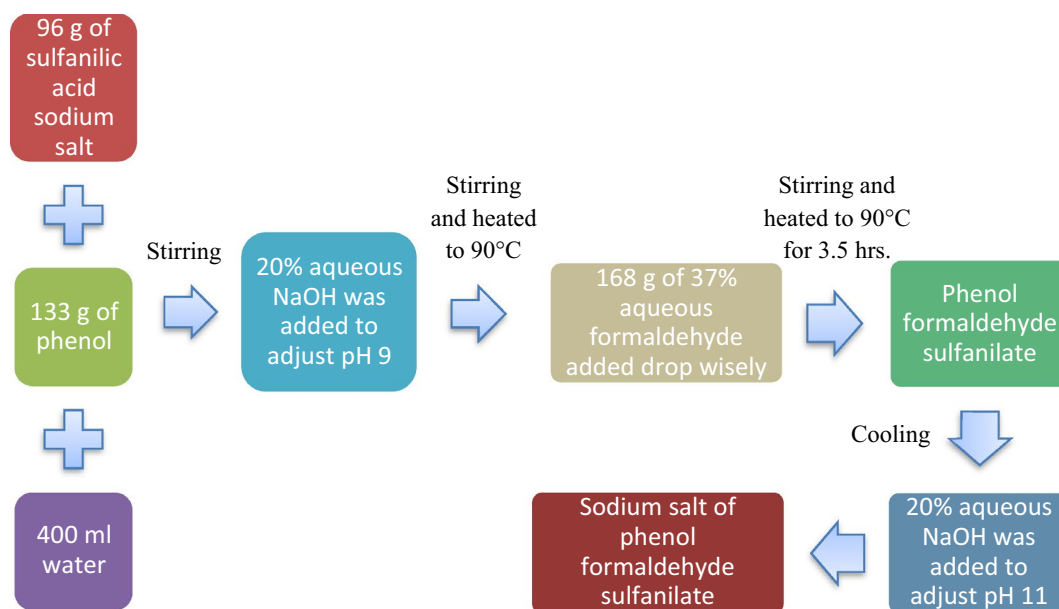
Fig. 2 Scheme form of the synthesized admixtures

Table 3 Physical properties of superplasticizers

Type	Color	Solid content (%)	Density (gm/ml)
Nb-SP	Brown liquid	42.50	1.09
PCb-SP	Reddish liquid	44.70	1.17
PFS-SP	Reddish brown	25.00	1.25

3 Experimental Program

3.1 Preparation Fresh Pastes

Firstly, the thermo-chemical-treated powders (TCT-P) were prepared using a thermo-chemical treatment technique. Each TCT-P contains 900 g GGBFS activated with 10 wt% NaOH (90 g). The preparation process passed through several stages: (i) 300 g GGBFS (one-third of total GGBFS weight) was mixed with 90 g grinded NaOH; (ii) the mix prepared in the first stage was sintered in a muffle furnace at different elevated temperatures (300 and 500 °C) for 2 h; (iii) the sintered process was followed by rapid cooling in the air; (iv) the powder obtained in the third stage was grinded to pass through 75 μm sieve; and (v) finally, the grinded powder was blended with the remaining amount of GGBFS (600 g) to attain a total weight of 900 g GGBFS.

To evaluate the effect of different SPs (Nb-SP, PCb-SP, PFS-SP) on the properties of one-part alkali-activated slag (OP-AAS), 14 mixes were designed as in Table 4. Different OP-AAS pastes were fabricated by mixing prepared TCT-Ps with water containing different dosages of SPs (0.00, 0.25 and 0.75 wt%) according to standard water

of consistency investigated by Vicat apparatus (ASTM C187-16) (Standard, 2016). The SPs were added to water, mixed in a mechanical stirrer for 30 s, and then mixed with the prepared TCT-P for 3 min at room temperature until a homogeneous mixture was obtained. Fig. 4 represents the preparation diagram of the mixes.

3.2 Testing Procedures

3.2.1 Mini Slump Test

The effect of different dosages from Nb-SP, PCb-SP, and PFS-SP on the flowability of OP-AAS pastes was evaluated using a mini-slump test (IOP, 2018; Habib et al., 2021; Ramadan et al., 2022b). The OP-AAS pastes were fabricated with a constant water/binder ratio equal to 0.6, mixed with different dosages SPs (0,00, 0.25, and 0.75 wt%). Then truncated cone (Abrams' cone) was filled with fresh paste; the top diameter of the cone is 19 mm, the bottom diameter is 38 mm and the height is 57 mm. Finally, the cone was raised vertically, and the paste's diameter was determined immediately in two perpendicular directions. Furthermore, the workability test was conducted on the OP-AAS mortar to increase the reliability of SPs' effect on fresh properties of OP-AAS. Therefore, the effect of adding 0.75 wt% from Nb-SP, PCb-SP, and PFS-SP on the workability of mortars fabricated from TCT-Ps at 300 and 500 °C was studied. The OP-AAS mortar was fabricated according to ASTM C109/C109M-20 (2020), in which the sand/binder ratio = 2.75 and the water/binder ratio = 0.55. According to ASTM C1437-20 (2020), the mortar
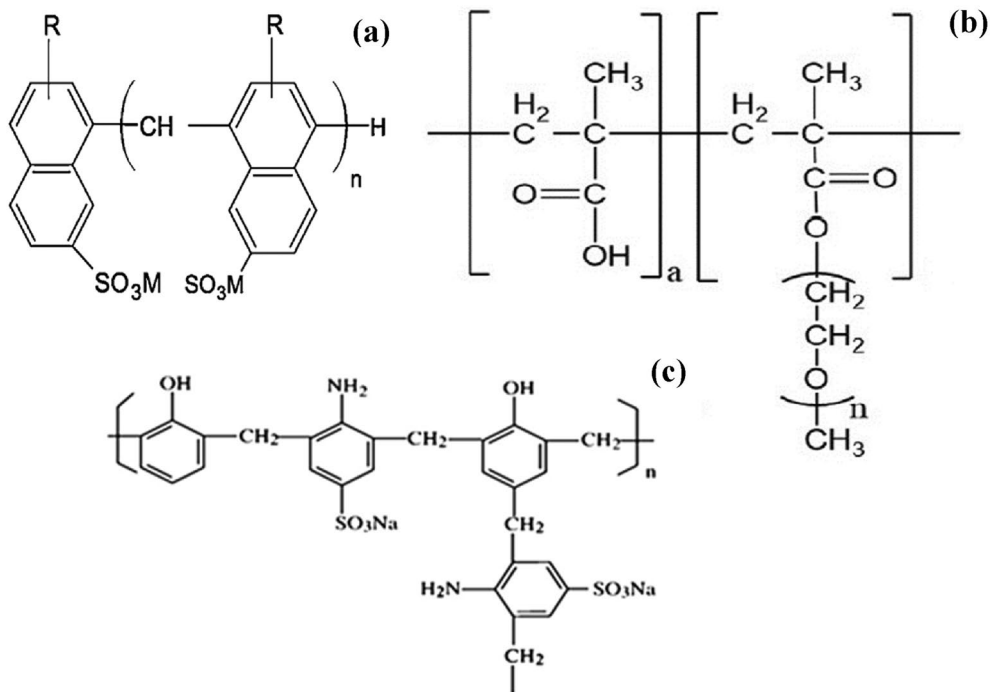
Fig. 3 Chemical structure of superplasticizers: **a** Nb-SP, **b** PCb-SP, and **c** PFS-SP

Table 4 Mixes preparation and design

Mix ID	Blended treated powder			Residual mixed slag g	Water/ binder ratio
	GGBFS (g)	NaOH (g)	Temp. (°C)		
OP300	300	90	300	600	0.35
OP300-N25					0.34
OP300-N75					0.31
OP300-PC25					0.35
OP300-PC75					0.33
OP300-PFS25					0.31
OP300-PFS75					0.31
OP500			500		0.35
OP500-N25					0.34
OP500-N75					0.33
OP500-PC25					0.35
OP500-PC75					0.33
OP500-PFS25					0.31
OP500-PFS75					0.31

was transferred to a truncated cone positioned in the center of the flow table. The truncated cone was lifted away from the mortar; the flow table dropped 25 times in 15 s, then the diameter was measured.

3.2.2 Setting Time Test
The initial and final setting times (I/F-ST) of each prepared OP-AAS paste were determined using the Vicat apparatus according to ASTM C191-19 (2019).
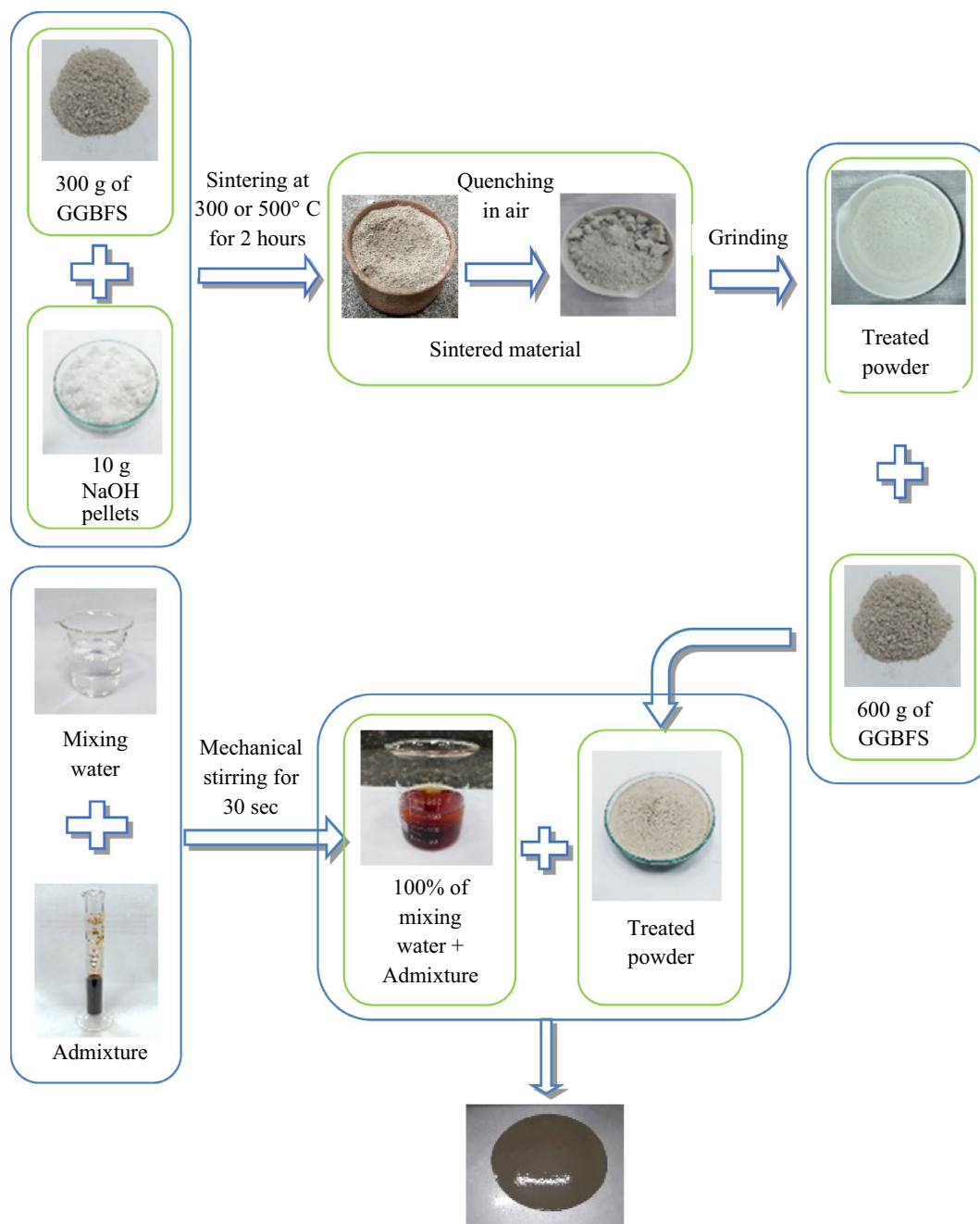
Fig. 4 Schematic diagram for the experimental program

3.2.3 Compressive Strength

The prepared pastes were poured into one-inch cubic molds and then vibrated on a vibrating table to obtain compact specimens. The specimens were cured in the humidifier (99% relative humidity) for 24 h at ambient temperature, then de-molded and cured at the same conditions till testing time. The progression in compressive strength with curing time (1, 3, 7, and 28 days) was measured in compliance with ASTMC109M-20b on the three specimens of each mix (ASTM, 2020).

3.2.4 Phase Composition

The phase composition of GGBFS before and after thermo-chemical treatment as well as after hydration was assessed by X-ray diffraction (XRD: Philips, model Xpert-2000) fitted with a scintillation detector has a power

of 40 mA and 40 kV (Cu-Kα = 1.5418 Å). The scanning range is 5–60° 2θ with a scan step time equal to 0.6 s/step and a step size equal to 0.02° 2θ.

4 Results and Discussion

4.1 Characterizations of Superplasticizers

The main effective function groups of SPs were detected through the FTIR test. Fig. 5 depicts the FTIR spectra of Nb-SP, PFS-SP and PCb-SP as well as Table 5 illustrates the band assignments. Regarding the Nb-SP, the presence of a band at 680 cm^{-1} associated with the S–O bond for sulfonic groups (SO_3^{2-}) was detected, which is the main functional group responsible for the creation of an electrostatic repulsion force between the grains of the binding material. The same band (680 cm^{-1}, SO_3^{2-})

was observed in the case of PFS-SP, which indicates that Nb-SP and PFS-SP have the same dispersion mechanism (electrostatic repulsion mechanism) (Gindy et al., 2022). In the case of PCb-SP, It was noticed that the presence of a band at 1457 cm^{-1} corresponding to the carboxylate groups and a band at 1636 cm^{-1} correlated to the C=O stretching bond of ester groups.

As illustrated above, molecular weight is one of the main factors affecting SPs' physical properties. Fig. 6 and Table 6 demonstrate the Mw, Mn and PDI values of SPs. It was observed that the Mw and Mn values of Nb-SP are higher than PFS-SP. Therefore, they are expected to have a different impact on the performance of building materials, although they have the same dispersion mechanism. Also, it was detected that the PCb-SP has the highest Mw
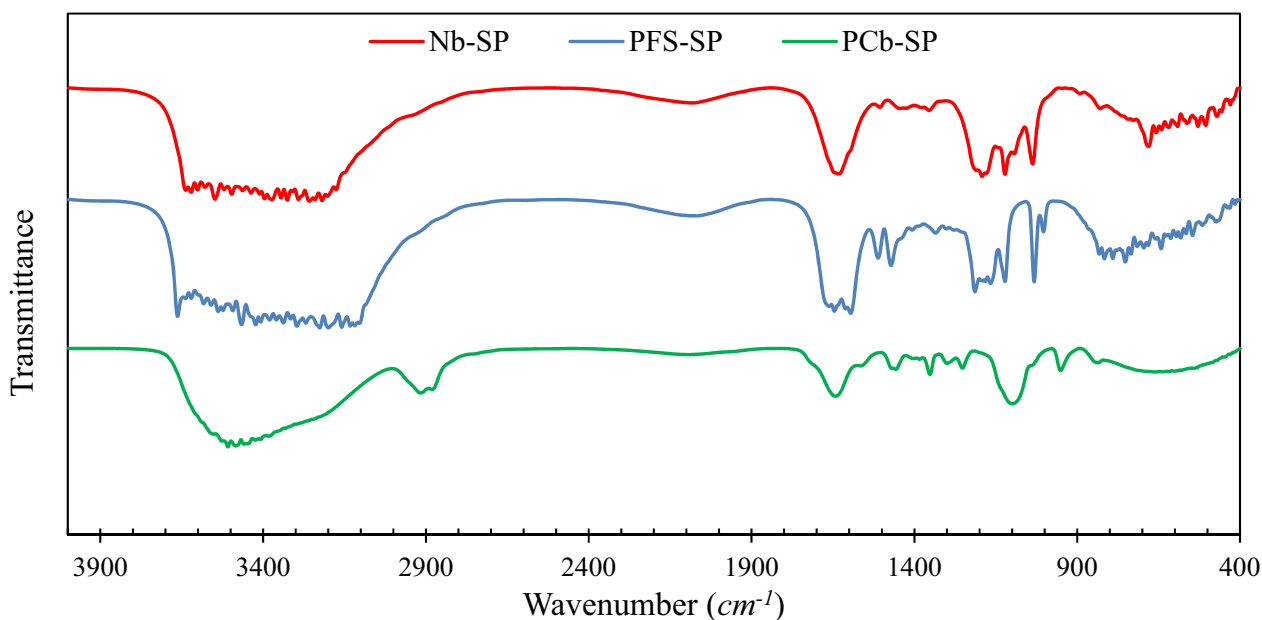

Fig. 5 FTIR-spectrum of the Nb-SP, PFS-SP and PCb-SP

Table 5 FTIR peak assignments for superplasticizers

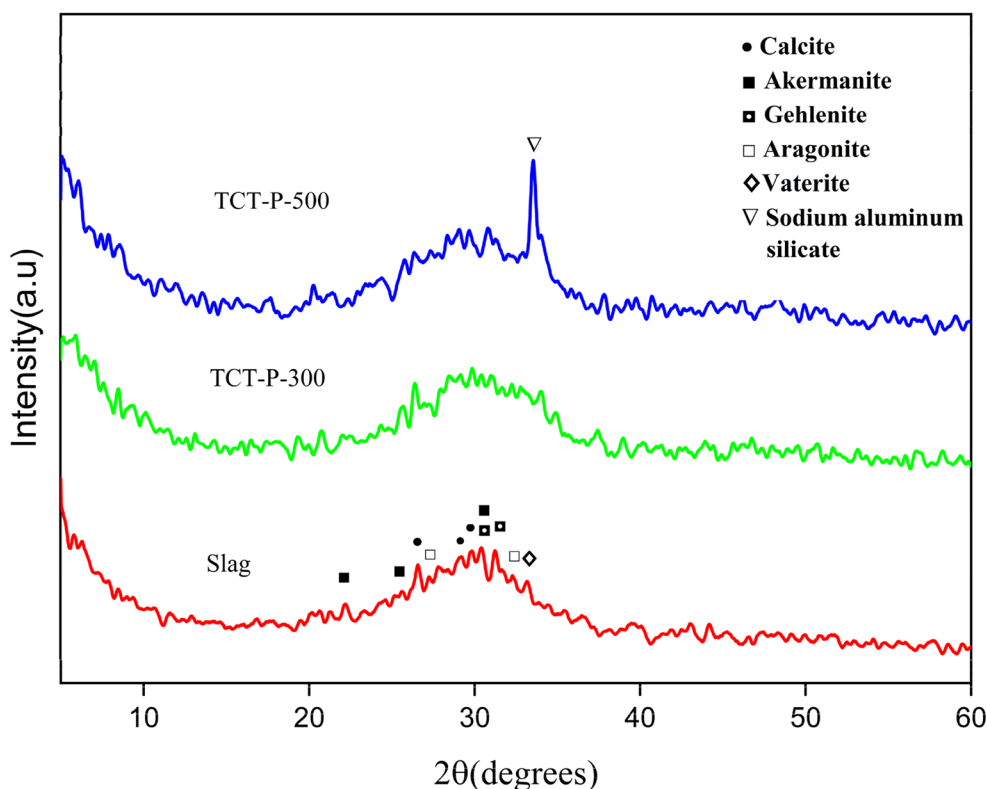| Wave number (cm^{-1})	Peak assignment	Type of superplasticizer related to peak assignment
3133–3663	O–H stretching	Nb-SP, PFS-SP and PCb-SP
3082	C–H stretching	PCb-SP
1636	C=O stretching (Ester group)	PCb-SP
1601, 1627 and 1646	C=C stretching	Nb-SP and PFS-SP
618, 1097 and 1352	C–O stretching	PCb-SP
1174	C–C stretching (aromatic)	Nb-SP
1038	C–H bending (–CH_2, –CH_3)	Nb-SP and PFS-SP
680	S–O deformation (–SO_3)	Nb-SP and PFS-SP
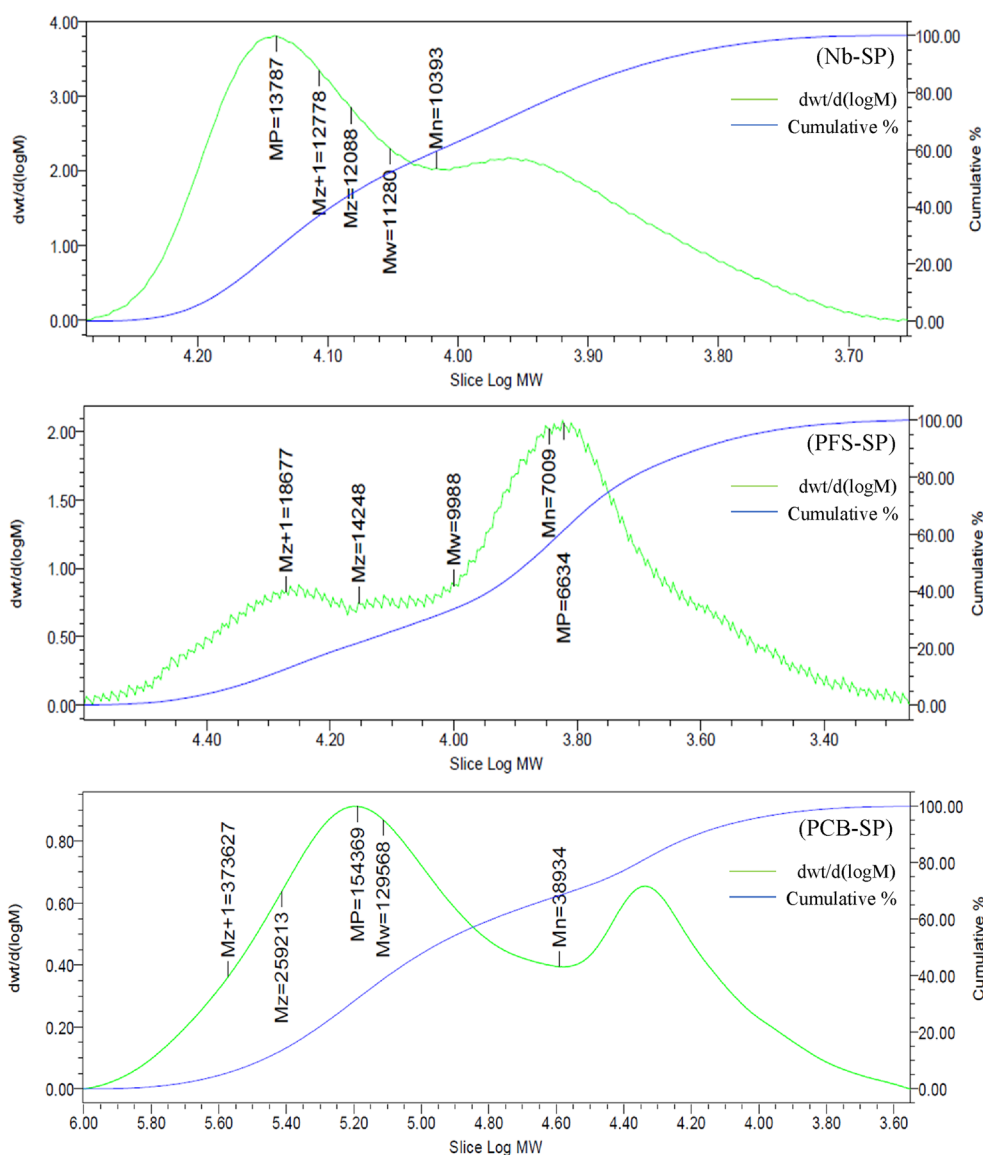
Fig. 6 GPC results of the Nb-SP, PFS-SP and PCb-SP

Table 6 Molecular weight and weight distribution of superplasticizers

Superplasticizer	Mw	Mn	PDI
Nb-SP	11,280	10,393	1.085
PFS-SP	9988	7009	1.425
PCb-SP	129,568	38,934	3.328

compared with Nb-SP and PFS-SP, indicating that it has long side chains, which are required for effective steric hindrance (Liu et al., 2194).

4.2 Characterizations of Thermo-chemical Treated Powder

The phase composition of the unhydrated GGBFS and thermo-chemical treated powder at 300 and 500 °C (TCT-P-300 and TCT-P-500) was examined using XRD, as displayed in Fig. 7. The XRD-pattern clarified the amorphous characteristics of GGBFS that are detected through a broad hump between 23.3 and 37.5° containing some poorly crystalline phases interrelated to akermanite at $2\theta = 22.3$, 25.7 and 30.47° (Ca_2Mg $[Si_2O_7]$, PDF# 01-079-2424), gehlenite at $2\theta = 30.47$ and 31.3° (Ca_2Al $[AlSiO_2]$, PDF# 01-079-2423), calcite at $2\theta = 26.6$, 29.3, 29.8 and 43.1° ($CaCO_3$, PDF# 01-071-3699), aragonite at $2\theta = 27.1$, 32.4 and 44.2° ($CaCO_3$,

Refaie *et al. Int J Concr Struct Mater*   (2023) 17:48

Page 10 of 22

Fig. 7 X-ray diffraction for raw materials

PDF# 01-076-0606) and vaterite at $2\theta = 33.2°$ ($CaCO_3$, PDF# 01-075-9356) (Ismail et al., 2014; Mohsen et al., 2020a; Ramadan et al., 2021).

As illustrated before, the main target of the thermochemical treatment process is impeding the NaOH in the aluminosilicate precursor structure to reduce its negative impact on the properties of AAS while using superplasticizers. The XRD analysis was employed to study the effect of thermal treatment temperature on the phase composition of TCT-P to identify the optimum conditions required to formulate safe powder to obtain OP-AAS with superior properties. Fig. 7 shows that the TCT-P-300 has an amorphousity approximately similar to GGBFS. The partial dissolution of akermanite and gehlenite phases in TCT-P-300 refers to its high reactivity, which may be resulting from the fluxing behavior of NaOH that depolymerize the crystalline structure of aluminosilicate precursor and then increase amorphousity (Abdel-Gawwad & Khalil, 2018; Abdel-Gawwad et al., 2018a, 2018b; Feng et al., 2012; Ramadan et al., 2021). Increasing the treatment temperature up to 500 °C (TCT-P-500) started the recrystallization of amorphous phases obtained above; furthermore, it led to the appearance of a new crystalline phase associated with sodium aluminum silicate phase at $2\theta = 33.5°$ ($Al_2Na_{1.84}O_{9.68}Si_{2.88}$,

PDF# 00-048-0731)), indicating the impeding of NaOH in the GGBFS structure. Nasr et al. (2018) observed a strong peak related to sodium calcium aluminum silicate (Na-rich anorthite, $Al_{1.8}Ca_{0.8}Na_{0.2}O_8Si_{2.2}$) at 200 °C in the XRD-pattern of AAS. When the temperature increased from 200 to 400 °C, the Na-rich anorthite phase transformed into the sodium aluminum silicate phase (Nasr et al., 2018).

4.3 Setting Time

Generally, a binding material must have a suitable setting time, which should not be very short to avoid the high heat resulting from the acceleration of the hydration process that leads to the evaporation of water and the formation of microcracks. On the other hand, the setting time must be long enough to allow for transportation and casting processes. As shown in Fig. 8, in the case of the control specimens (OP300 and OP500), it was found that an increase in the sintered temperature is accompanied by an elongation of the setting time. This may be attributed to the strengthening of the bond between Na_2O and aluminosilicate precursors with increasing sintered temperature, which delays the alkaline activation process (Mohammed et al., 2019). Additionally, due to the relatively high crystallinity of the TCT-P-500 rather than
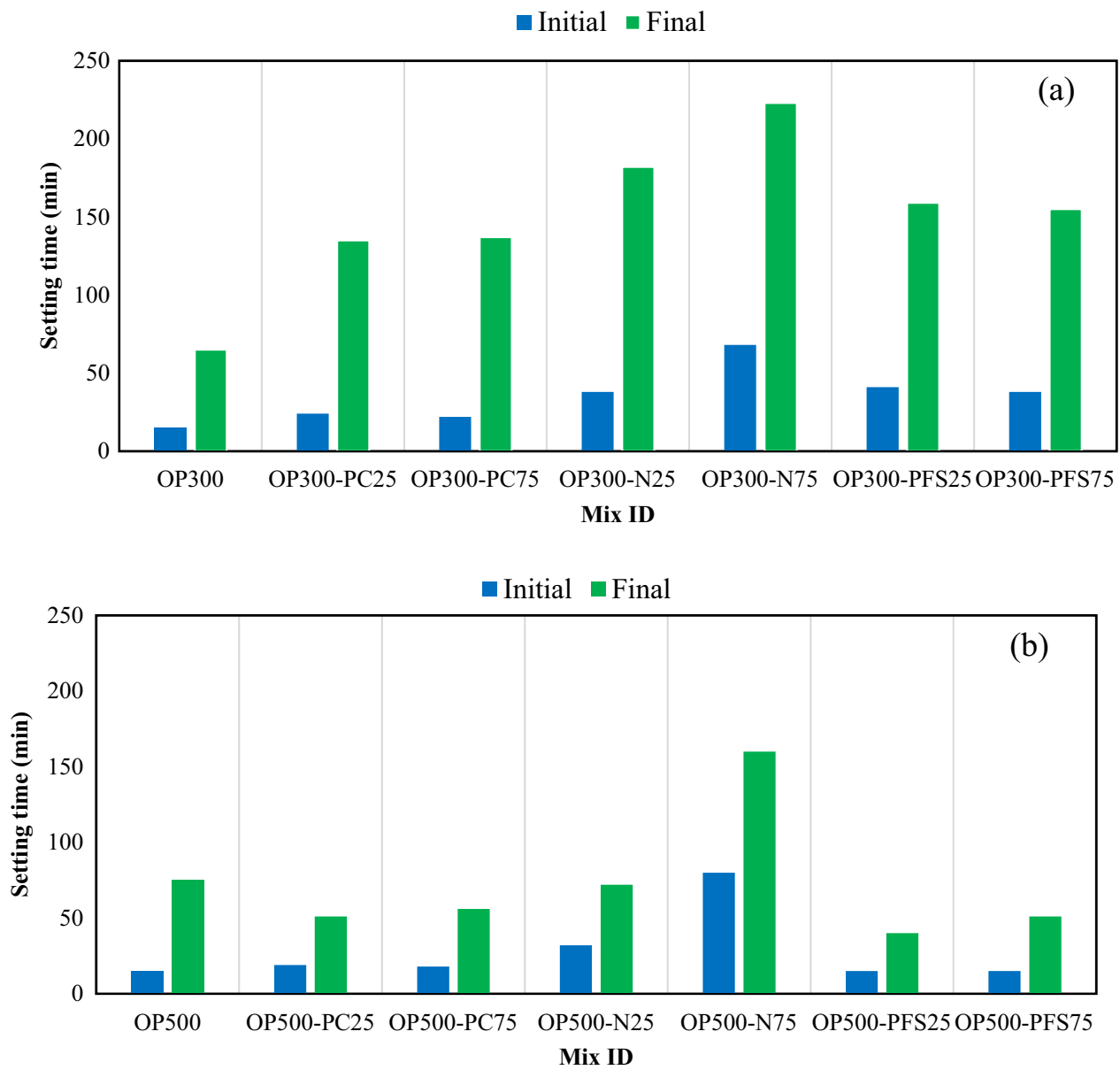
Fig. 8 Impact of superplasticizers on the setting time values of pastes prepared from **a** TCT-P-300, **b** TCT-P-500

TCT-P-300 (TCT-P-500 is less reactive than TCT-P-300), the setting time in OP500 was delayed.

On the contrary, in the case of admixed pastes (presence SPs), it is noteworthy to observe that the setting time in pastes prepared from TCT-P-300 is longer than at 500 °C. It is expected that the mean reason behind this phenomenon is the adsorption efficiency of the SPs on the TCT-P. As discussed previously, the dissolution process of TCT-P-300 was faster than at TCT-P-500, meaning that the amount of Ca^{2+} ions adsorbed on the deprotonated Si–OH was higher at 300 °C. This refers to the strong adsorption of SPs on the TCT-P-300 rather than the TCT-P-500. Therefore, the retardation effect at 300 °C may be rising from the adsorption of SPs on the TCT-P grains (Zingg et al., 2009), forming a semipermeable film (protective film) (Bishop & Barron, 2006; Bullard et al., 2011; Marchon & Flatt, 2016a; Möschner et al., 2009), resulting in closing the open pits required for further dissolution process. Opening pits is important for reaching the water to the anhydrous phases to allow continuous alkaline activation.

Blocking these pits delayed the activation process for a certain time (Juilland et al., 2010).

Fig. 8 represents that the retardation effect of Nb-SP was more significant than PFS-SP and PCb-SP in the pastes prepared from TCT-P-300 and TCT-P-500. Regarding PFS-SP, the Nb-Sb has a higher Mw and Mn than PFS-SP, leading to the formation of a thick layer around TCT-P, blocking the pits and then retarding the setting time. Regarding PCb-SP, owing to the high stability and strong adsorption of Nb-SP in an alkaline medium than PCb-SP, the setting time was elongated. At 300 °C, the retardation effect of the PFS-SP was higher than PCb-SP due to the low adsorption of PCb-SP than PFS-SP that is resulting from competitive adsorption between PCb-SP and OH^- group (Marchon & Flatt, 2016b; Marchon et al., 2013). The high anionic charge density of polycondensate SPs as Nb-SP is the purpose behind its high adsorption than polycarboxylates (PCb-SP) (Lei & Chan, 2020; Lei & Zhang, 2021; Plank & Hirsch, 2007). At 500 °C, there was no retardation effect for both PFS and PCb-SPs, which resulted from (i) low adsorption due to low Ca^{2+} ions beside low Mw and Mn in the case of PFS-SP; and (ii) very low adsorption owing to competence with OH-group beside limiting the amount of Ca^{2+} ions required for adsorption in the case of PCb-SP.

4.4 Mini Slump

Workability is an important characteristic that describes the mixing, placing and consolidating of fresh paste to design suitable mixer and pump equipment. The effect of sintered temperature on the workability of fabricated fresh pastes is shown in Fig. 9. Generally, it was detected that increasing the sintered temperature led to enhancing the workability. At 300 °C, the TCT-P shows a high amorphousity as approved above by XRD analysis that means (i) absorb a high amount of free water; and (ii) weakly attached Na_2O to aluminosilicate precursor that becomes free to participate in the alkaline activation process (Refaat et al., 2021). On the other hand, increasing the treatment temperature up to 500 °C led to increasing the degree of crystallinity and then improving workability (Jamil et al., 2021). This may be attached to the fact that the less reactivity of crystalline materials than amorphous ones results in decreasing water consumption and lowering the rate of hydration due to impeding Na_2O required for the alkaline activation process in the aluminosilicate structure, making a sufficient amount of free water available to improve workability (Mohammed et al., 2019; Neupane, 2016; Walker & Pavía, 2011).

Commonly, improving cement flowability in the presence of SPs is described by their adsorption on the surfaces of cement particles, which prevents flocculation and coalescence. As a result, the uniform distribution of cement particles reduces the amount of trapped water, making more free water available for improving workability and allowing water to reach the cement surface, aiding the hydration process. The dispersion phenomena of SPs are mostly dependent on their chemical structure. There are many mechanisms correlated to enhancing the workability of binding materials in the presence of SPs that are (i) changing in water surface tension; (ii) forming of layers around cement particles that delay the hydration process and allow more free water to be used to enhance the workability; (iii) creating of a lubricating film between particles; (iv) establishing of an electrostatic repulsion force on the cement particles; and (v) constructing of steric hindrance between particles (Puertas et al., 2003; Ramachandran et al., 1998). Because cement and alkali-activated slag have different physical and chemical properties, morphology, and alkalinity, their dispersion phenomena of superplasticizers behave differently (Puertas et al., 2003). In the alkali-activated slag, the high alkalinity medium (high pH value) leads to deprotonation of the silanol group (Si–OH) from the aluminosilicate structure, leaving a negative charge on the GGBFS grains (Habbaba & Plank, 2010, 2012). With time, the dissolution of GGBFS particles results in releasing of cation species (Ca^{2+} ions), which then attach to deprotonated Si–OH (negative spots), allowing the existence of positively charged sites and then creating a double-layer structure (DLVO theory) (Boström et al., 2006; Kashani et al., 2014; Labbez et al., 2006). The anionic SPs adsorbed on the Ca^{2+} ions (positively charged sites) (Ohta et al., 1997; Yoshioka et al., 1997), creating a repulsive force between grains, resulting in particle separation and enhancing workability. Therefore, the effect of different dosages (0.25 and 0.75 wt%) of various SPs (Nb-SP, PCb-SP, and PFS-SP) on the flowability behavior of fresh pastes was studied.

Fig. 9a displays the effect of Nb-SP, PCb-SP, and PFS-SP on the workability of fresh pastes prepared from TCT-P-300. It was observed that all dosages from SPs caused an increase in workability except 0.25 wt% from PCb-SP (OP300-PC25) decreased the workability by 45%. The spread area of OP300-N25, OP300-N75, OP300-PFS25, and OP300-PFS75 increased by 39, 54, 34 and 62%, respectively, than OP300 (0 wt% SPs) due to the high stability Nb-SP and PFS-SP in an alkaline medium which resulting from their aromatic nature (Meletov, 1991). The negative impact of low dosages from PCb-SP (0.25 wt%) may be explained by its instability in a highly alkaline medium; therefore, it partially decomposed into a carboxylic acid and respective ether in the bulk solution leading to an increase in the viscosity (Palacios et al., 2003). Although the thermal treatment process, the TCT-P-300 has high alkalinity, as a high amount of free NaOH
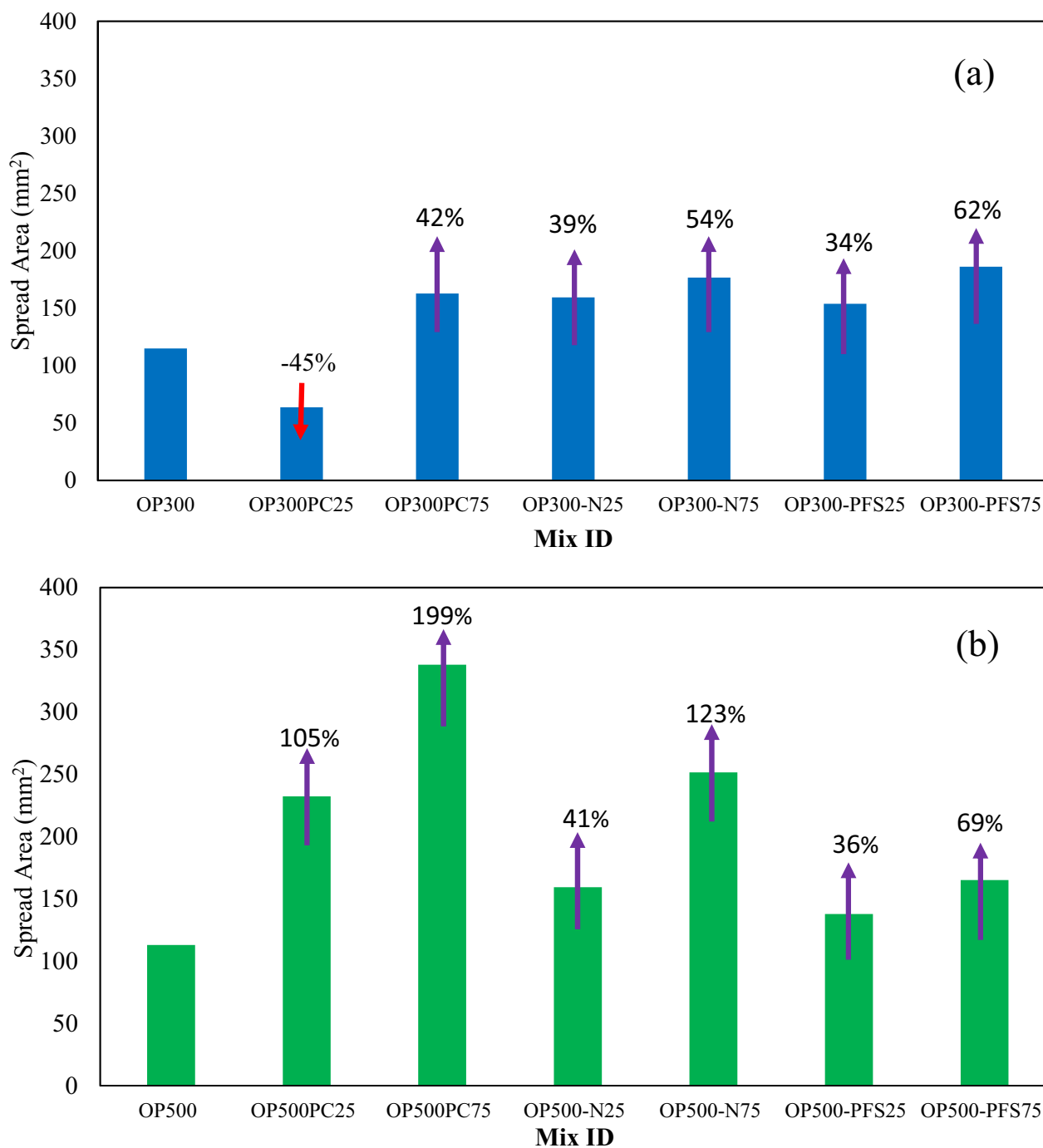
Fig. 9 Impact of superplasticizers on the spread area values of pastes prepared from **a** TCT-P-300, **b** TCT-P-500

pallet is not impeded in aluminosilicate precursors (the melting point of NaOH is 318 °C). Also, the PCb-SP negative effect may be attributed to competitive adsorption between the OH^- group and PCb-SP (Marchon et al., 2013, 2016a). At higher PCb-SP dosage (0.75 wt%), the

workability was enhanced by 42% due to the availability of a sufficient long chain of PCb-SP caused steric hindrance (Lei & Chan, 2020; Yahia, 2011).

Fig. 9b shows that PCb-SP significantly enhanced the workability of pastes fabricated from TCT-P-500

compared to the Nb-SP and PFS-SP (0.25 and 0.75 wt% increased the spread area by 105 and 199%, respectively). At 500 °C, most NaOH impeded in the aluminosilicate precursors, decreased the alkalinity, prevented hydrolysis of PCb-SP and then allowed it to work as efficiently as in cement. The high efficiency of PCb-SP resulted from its high dispersion effect by electrostatic repulsion force and steric hindrance (3rd generation SP) (Ren, 2016; Yamada et al., 2000). This phenomenon shows the importance of the thermochemical treatment process in using the available SPs in the market. Fig. 10 shows the impact of 0.75 wt% from Nb-SP, PCb-SP and PFS-SP on the workability of mortars prepared from TCT-P-300 and TCT-P-500. It was noticed that the effect of these superplasticizers on the workability of the pastes and mortars has the same trend. All admixed mortars fabricated from TCT-P-500 have workability higher than TCT-P-300; adding PCb-SP, Nb-SP and PFS-SP to the TCT-P-300-based mortar increased the spread area by 44, 60 and 70.1% the control specimen (TCT-P-300-based mortar without admixtures), while adding the same admixtures to TCT-P-500-based mortar increased the spread area by 131.6, 81.6 and 73.5% the control specimen (TCT-P-500-based mortar without admixtures), respectively. Also, it was observed that the instability problem of 3rd generation SP (PCb-SP) can be solved by employing the thermo-chemical treatment in the preparation of one-part alkali-activated materials, as illustrated above.
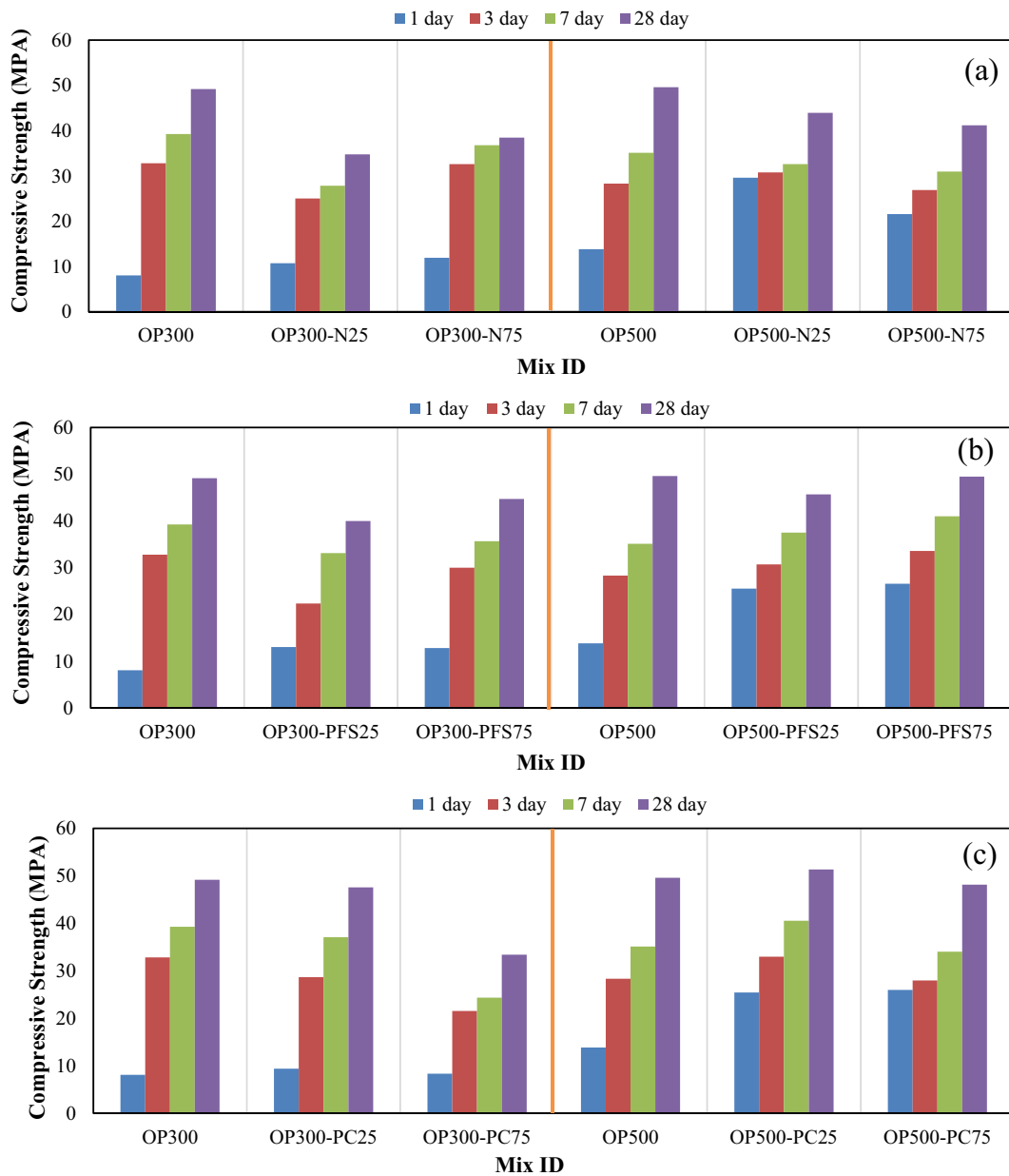
4.5 Compressive Strength

The effect of various dosages (0.00, 0.25 and 0.75 wt%) from different SPs (Nb-SP, PFS-SP and PCb-SP) on the mechanical compressive strength (MCS) of hardened pastes fabricated from TCT-P-300 and TCT-P-500 is demonstrated in Fig. 11. Generally, it was detected that the increasing the curing period (from 1 to 28 days) is accompanied with a significant progression in MCS values for all mixes, which may be attributed to a continuous alkaline activation process that resulted in the invention of an enormous amount of binding phases [calcium-silicate-hydrate (C-S-H) and calcium-aluminosilicate-hydrate (C-A-S-H)] that fill the pores between grains (Ismail et al., 2014; Li et al., 2010; Mohsen et al., 2022c; Puertas et al., 2011; Shwita et al., 2021).

From Fig. 11a, it was concluded that the addition of Nb-SP has a negative impact on the MCS value for all hardened pastes prepared from TCT-P-300 and TCT-P-500. This may be traced back to the retardation effect of the Nb-SP. Adsorption of Nb-SP (retarder SP) on the unreacted grains and/or hydration products causes blocking of the open pits and poising the nuclei required for alkaline activation reaction progress, leading to inhibit growth further binding phases and then reduces the MCS (Marchon & Flatt, 2016b; Marchon et al., 2016b). Furthermore, several studies revealed that the retarder SPs lead to the existence of a high amount of free water (not participating in the hydration process) that can evaporate, causing the plastic shrinkage
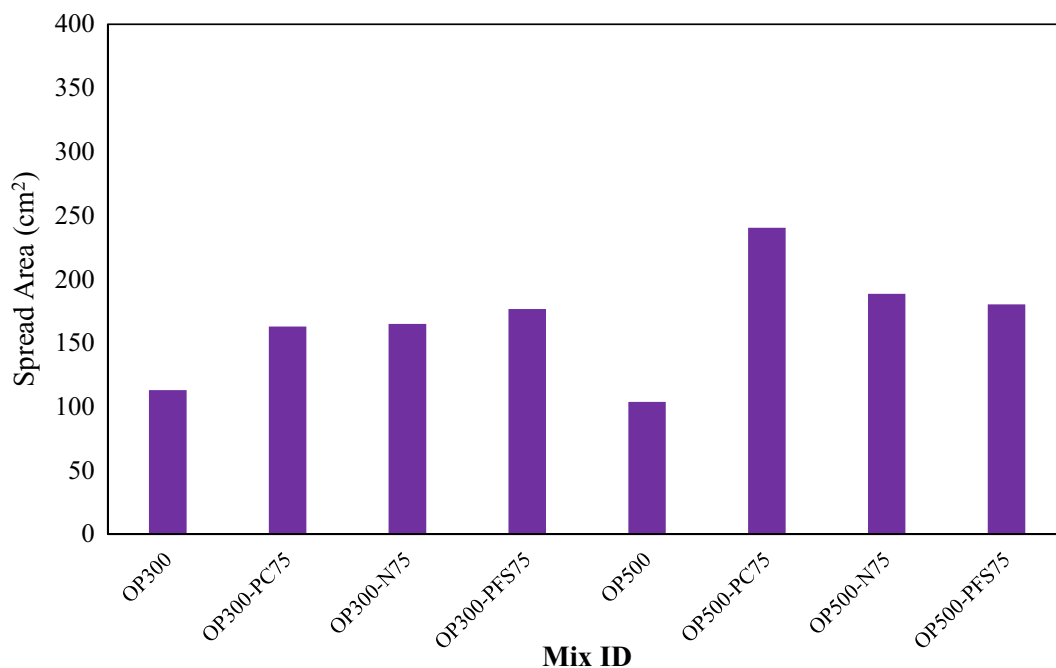
Fig. 10 Impact of superplasticizers on the spread area values of mortars prepared from TCT-P-300 and TCT-P-500

Fig. 11 Compressive strength values for pastes admixed with different dosages from **a** Nb-SP, **b** PFS-SP, **c** PCb-SP

risk (formation of microcracks) and then decreasing the MCS (Esping & Löfgren, 2005; Soroka, 1993; Zuhua et al., 2009). Also, the evaporation process makes water present insufficient to complete the alkaline activation reaction (Mohsen et al., 2020b). The MCS of admixed pastes prepared from TCT-P-500 °C is higher than 300 °C due to the reduction in the retardation effect at 500 °C as illustrated above. At 300 °C, as the dosage of Nb-SP increased, the MCS value increased due to the reduction in the water of consistency by 8.8% when the dosage of Nb-SP increased from 0.25 to 0.75 wt%. The reduction in

the water of consistency decreases the pore size; therefore, the least amount of hydration products can fill the pores (high gel/space ratio), giving a compact structure and causing an enhancement in MCS (Mohsen et al., 2020b). At 500 °C, both OP500-N25 and OP500-N75 have approximately similar MCS values, as there is no significant difference in the water of consistency (water/binder ratio = 0.34 and 0.33 for OP500-N25 and OP500-N75, respectively).

Also, from Fig. 11b, it was observed that adding PFS-SP reduced the MCS of pastes prepared from TCT-P-300; at

28 days, the MCS decreased by 18.6 and 9.1% for OP300-PFS25 and OP300-PFS75, respectively, compared to OP-300. This may result from the retardation effect of PFS-SP that has a negative impact on the MCS (plastic shrinkage and hydration nuclei poising), as discussed above. Interestingly, the PFS-SP improved the MCS for AAS prepared from TCT-P-500, especially up to 7 days of hydration, due to the acceleration effect of PFS-SP that solves most of the retardation problems illustrated above. Besides the acceleration effect, decreasing the water/binder ratio by 8.8% increased the gel/space ratio and then enhanced the MCS values. As the dosage of PFS-Sb increased, the MCS increased. The appropriate workability resulted from a high dosage PFS-SP caused redistribution of pore structure followed by reducing capillary stress and increasing MCS (Palacios & Puertas, 2007). Furthermore, PFS-SP may reduce the surface tension of mixing water, limiting its evaporation and then reducing shrinkage (Folliard & Berke, 1997).

Fig. 11C shows that the PCb-SP has a detrimental impact on the MCS of pastes synthesized from TCT-P-300 due to the same reasons illustrated above. Also, it was noticed that increasing the dosage of PCb-SP from 0.25 to 0.75 wt% reduced the MCS of OP300-PC75 by 29.8% more than OP300-PC25 at 28 days. This is probably due to consuming a high amount of free NaOH required to continue the alkaline activation process in the

hydrolysis of PCb-SP. In the case of TCT-P-500, the MCS was enhanced than pastes prepared from TCT-P-300 due to its acceleration effect and enhancement in workability at 500 °C. OP500-PC25 showed a higher MCS than OP500-PC 75, which can be attributed to the high workability that can bleed free water on the specimen's surface, which is easily scraped, referring to decreasing in the MCS (Collins & Sanjayan, 1998).

4.6 Mineralogical Analysis Through XRD

The effect of adding 0.25 wt% from different SPs (Nb-SP, PFS-SP and PCb-SP) on the phase composition of hardened pastes fabricated from TCT-P-300 and TCT-P-500 at 1 and 28 days was studied using XRD analysis as shown in Figs. 12, 13 and 14. The XRD-pattern for specimens admixed with Nb-SP (Fig. 12) cured for 1 day showed a broad hump between $2\theta = 26°-33°$ centered at $2\theta = 29.4°$, referring to the formation of ill-crystalline to amorphous hydration products such as tobermorite gel (C–S–H, $(CaO)_{1.7}(SiO_2)(H_2O)_{1.8}$, PDF# 00-033-0306 and 00-034-0002) and Al-tobermorite gel (C–A–S–H, $(CaO)_{1.7}(Al_2O_3)_{0.05}SiO_2(H_2O)_{1.9}$, PDF# 00-020-0452), which are responsible for enhancing the mechanical properties (Nasir et al., 2020; Ramadan et al., 2021). Also, some diminished peaks associated with the presence of crystalline phases were noticed, such as (i) hydrotalcite $(Mg_6Al_2(CO_3)(OH)_{16}.4(H_2O)$, PDF# 00-041-1428)
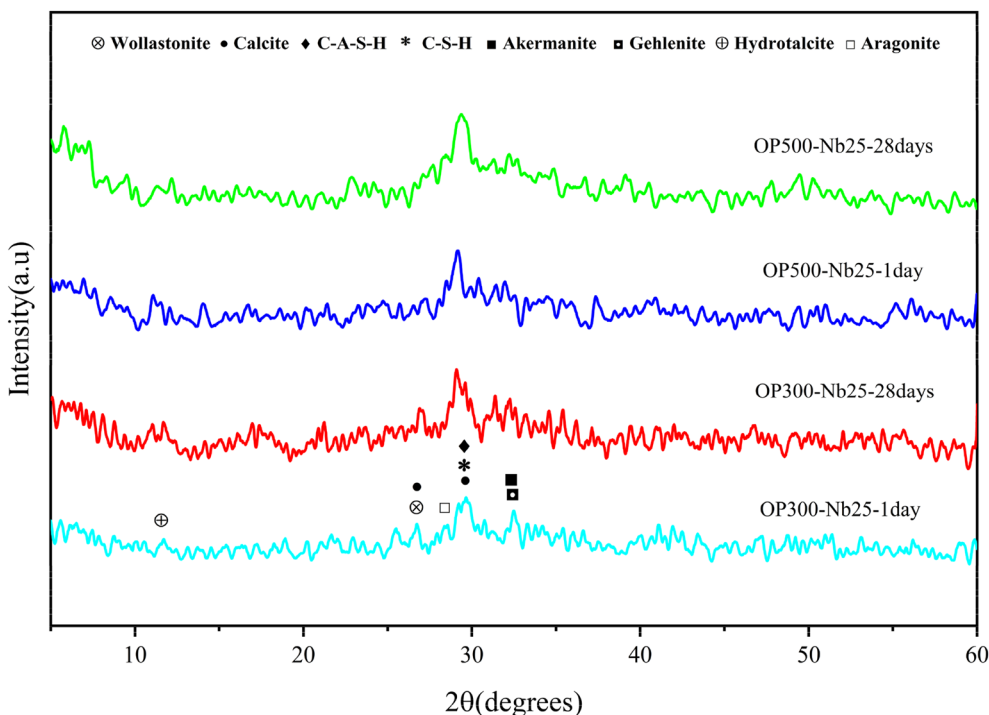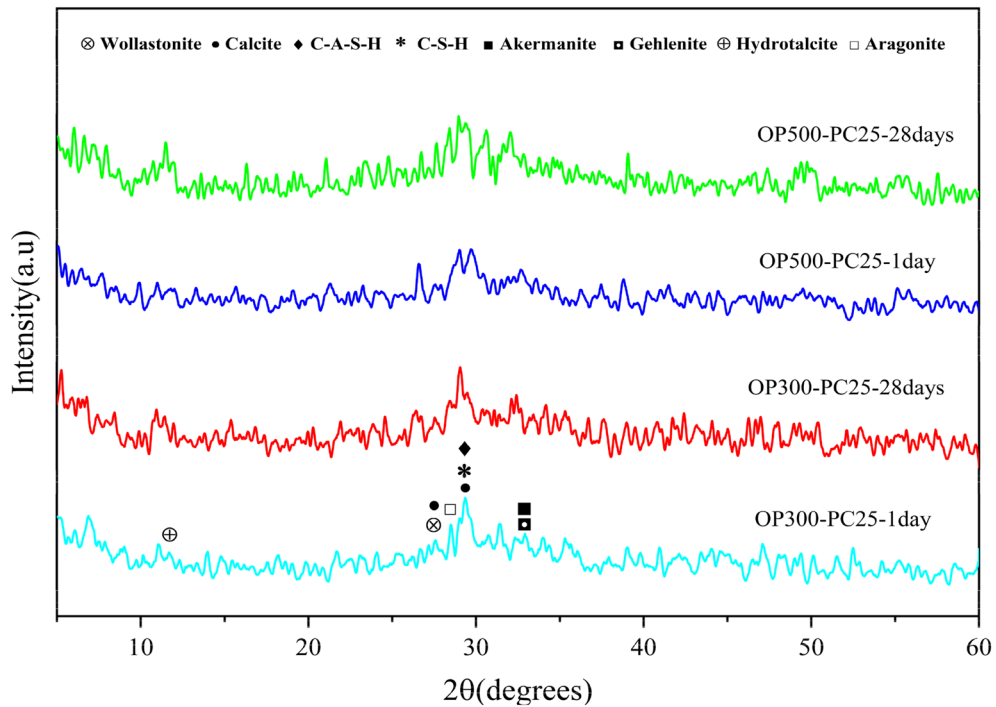

Fig. 12 XRD-pattern for hardened pastes admixed with Nb-SP at 1 and 28 days
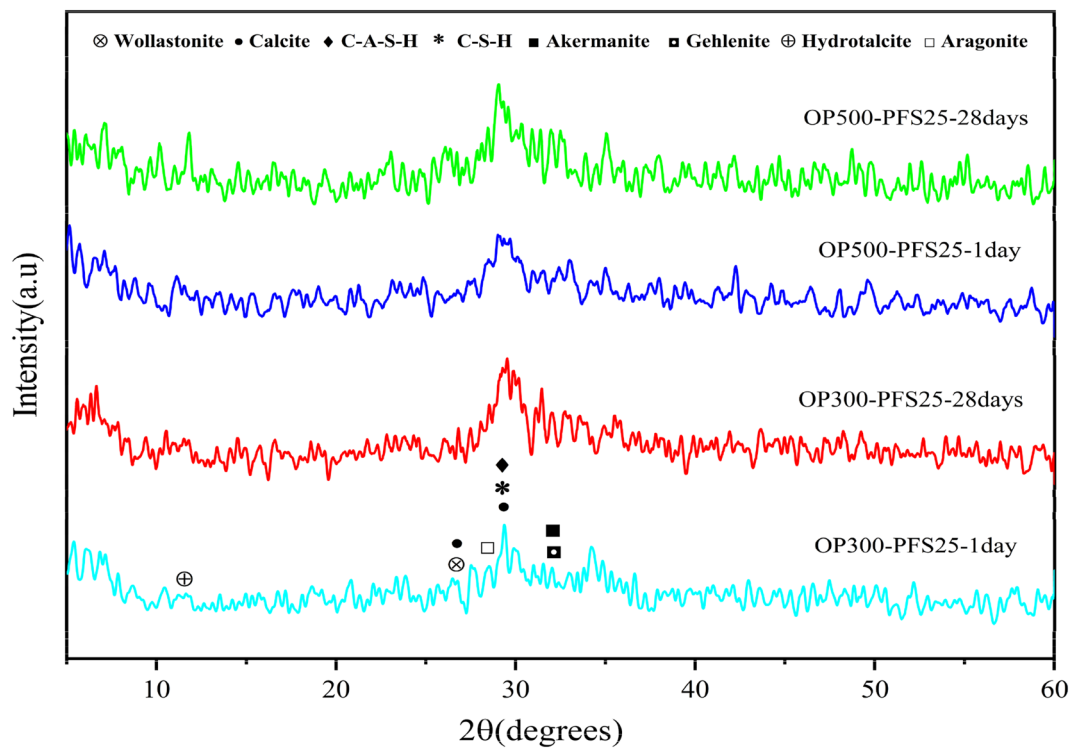
Fig. 13 XRD-pattern for hardened pastes admixed with PFS-SP at 1 and 28 days

Fig. 14 XRD-pattern for hardened pastes admixed with PCb-SP at 1 and 28 days

Refaie *et al. Int J Concr Struct Mater*   (2023) 17:48

Page 18 of 22

at $2\theta = 11.7°$ (Mohsen et al., 2020a; Oh et al., 2010), (ii) wollastonite (CaSiO$_3$, PDF# 00-029-0372) at $2\theta = 26.7°$ (Mohsen et al., 2020a, 2021), (iii) aragonite (CaCO$_3$, PDF# 01-076-0606) at $2\theta = 28.5°$ (Ismail et al., 2014), (iv) calcite at $2\theta = 26.7$ and $29.6°$ (CaCO$_3$, PDF# 01-071-3699) (Ismail et al., 2014; Ramadan et al., 2022a) (v) gehlenite (Ca$_2$Al [AlSiO$_2$], PDF# 01-079-2423) and akermanite (Ca$_2$Mg [Si$_2$O$_7$], PDF# 01-079-2424) and at $2\theta = 32.4°$ (Mohsen et al., 2020a, 2021). It was noticed that all admixed specimens have the same peaks with different intensities, which indicates that the SPs do not affect the phase composition. Therefore, the main reason behind the difference in the MCS values is the alternating effect of SPs on the physical properties of binding materials, such as water/binder ratio, workability and setting time (Habib et al., 2016, 2018; Mohsen et al., 2020b). Also, for all admixed specimens with Nb-SP, PFS-SP and PCb-SP, the same phases illustrated above had been identified at 28 days of hydration. Increasing the intensities of tobermorite and Al-tobermorite phases (main hydration products) and decreasing the intensities of gehlenite and akermanite (unreacted phases of GGBFS) refers to continuous activation of unreacted phases, which can explain the enhancement of MCS with the curing time (Ramadan et al., 2021). By comparing the intensities of the peaks affiliated with hydration products in the specimens prepared from TCT-P-300 and TCT-P-500, it was detected that the intensities of the peaks in the case of OP500-N25, OP500-PFS25 and OP500-PC25 are higher than OP300-N25, OP300-PFS25 and OP300-PC25, respectively, which is strongly correlated to the MCS results (The MCS values of admixed OP-AAS prepared from TCT-P-500 is higher than TCT-P-300). The low peaks' intensities of admixed OP300 than OP500 may be assigned to the high retardation effect for Nb-SP and PFS-SP in the TCT-P-300 that caused evaporation of most of the water needed for the hydration reaction, also due to consumption a high amount of free NaOH necessary for alkaline activation process in the hydrolysis of PCb-SP.

5 Conclusion

This study demonstrates the impact of different dosages (0.25 and 0.75 wt%) of three superplasticizers (modified naphthalene-based (Nb-SP), modified polycarboxylate-based (PCb-SP) and phenol formaldehyde sulfanilate (PFS-SP)) on the properties of OP-AAS prepared from thermo-chemical treatment process at 300 and 500 °C. From the above results, the following points can be concluded:

- Utilizing the thermal treatment process in fabricating OP-AAS is an effective method for mitigating the effect of the highly alkaline medium by impeding the NaOH in the aluminosilicate precursor structure. This was clarified by forming the sodium aluminum silicate phase after sintering a mixture from GGBFS with 10 wt% NaOH at 500 °C, as identified by XRD.

- The thermo-chemical treatment process will become a promising way to solve the problem of using chemical admixtures in alkali-activated materials by allowing the use of superplasticizers available in the market. This was inferred from the workability and compressive strength results.

- Increasing the sintering temperature improved the workability of all admixed OP-AAS. Laboratory-prepared superplasticizer (PFS) showed the highest enhancement percentage in workability in the case of OP-AAS prepared from TCT-P at 300 °C, which refers to its high stability in the highly alkaline medium.

- In the TCT-P prepared at 500 °C, PCb-SP enhanced the workability by 199%, which clarified the role of the thermal treatment process in limiting the hydrolysis of the polycarboxylate polymer. This is the biggest evidence that the commercial PCb-SP can operate in OP-AAS (prepared from TCT-P-500) with the same efficiency as in Portland cement.

- Nb-SP has the highest retardation impact on the OP-AAS fabricated from TCT-P-300 and TCT-P-500, referring to its strong adsorption on the binder grains. The main reasons for Nb-SP's adsorption are the high molecular weight and high anionic charge density than PFS-SP and PCb-SP, respectively.

- Nb-SP negatively impacts the mechanical properties, while OP-AAS, admixed with PFS and PCb-SPs, demonstrated the highest compressive strength values.

- In this work, a radical solution to the problem of using SPs in alkali-activated materials was found by using an invented laboratory-prepared SP (PFS-SP) and commercial superplasticizer (PCb-SP).

Abbreviations

AAM	Alkali-activated materials
AAS	Alkali-activated slag
TP	Two-part
OP	One-part
SP	Superplasticizer
GGBFS	Ground granulated blast furnace slag
Nb-SP	Naphthalene-based superplasticizer
PCb-SP	Polycarboxylate-based superplasticizer
PFS-SP	Phenol formaldehyde sulfanilate superplasticizer
TCT-P	Thermo-chemical-treated powder
C-S-H	Calcium-silicate-hydrates
CASH	Calcium-alumino-silicate-hydrate
XRF	X-ray fluorescence

XRD   X-ray diffraction
FTIR   Fourier transform infrared
GPC   Gel permeation chromatography
Mw   Weight average molecular weight
Mn   Number average molecular weight
PDI   Polydispersity index
I/F-ST   Initial/final setting time
MCS   Mechanical compressive strength

Author contributions
MR: methodology, investigation, writing—original draft. AM: conceptualiza-tion, investigation, methodology, writing—original draft, writing—review and editing, visualization, resources. E-SN: supervision. MK: conceptualization, methodology, writing—review and editing, resources, supervision, project administration. All authors read and approved the final manuscript.

Availability of data and materials
All data generated or analyzed during this study are included in this published article.

Declarations

Competing interests
No competing interests exist in the submission of this manuscript, and manu-script is approved by all authors for publication. The author declares that the work described was original research that has not been published previously, and not under consideration for publication elsewhere.

References
Abdel-Gawwad, H. A., García, S. R. V., & Hassan, H. S. (2018a). Thermal activation of air cooled slag to create one-part alkali activated cement. *Ceramics International, 44*, 14935–14939. https://doi.org/10.1016/j.ceramint.2018.05.089

Abdel-Gawwad, H. A., Heikal, E., El-Didamony, H., Hashim, F. S., & Mohammed, A. H. (2018b). Recycling of concrete waste to produce ready-mix alkali activated cement. *Ceramics International, 44*, 7300–7304. https://doi.org/10.1016/j.ceramint.2018.01.042

Abdel-Gawwad, H. A., & Khalil, K. A. (2018). Application of thermal treatment on cement kiln dust and feldspar to create one-part geopolymer cement. *Construction and Building Materials, 187*, 231–237. https://doi.org/10.1016/j.conbuildmat.2018.07.161

Abed, M. H., Abbas, I. S., Hamed, M., & Canakci, H. (2022). Rheological, fresh, and mechanical properties of mechanochemically activated geopolymer grout: A comparative study with conventionally activated geopolymer grout. *Construction and Building Materials, 322*, 126338. https://doi.org/10.1016/J.CONBUILDMAT.2022.126338

Alrefaei, Y., Wang, Y.-S., & Dai, J.-G. (2019). The effectiveness of different super-plasticizers in ambient cured one-part alkali activated pastes. *Cement and Concrete Composites, 97*, 166–174. https://doi.org/10.1016/J.CEMCONCOMP.2018.12.027

Alrefaei, Y., Wang, Y. S., Dai, J. G., & Xu, Q. F. (2020). Effect of superplasticizers on properties of one-part Ca(OH)$_2$/Na$_2$SO$_4$ activated geopolymer pastes. *Construction and Building Materials, 241*, 117990. https://doi.org/10.1016/J.CONBUILDMAT.2019.117990

Askarian, M., Tao, Z., Adam, G., & Samali, B. (2018). Mechanical properties of ambient cured one-part hybrid OPC-geopolymer concrete. *Construction and Building Materials, 186*, 330–337. https://doi.org/10.1016/j.conbuildmat.2018.07.160

Askarian, M., Tao, Z., Samali, B., Adam, G., & Shuaibu, R. (2019). Mix composition and characterisation of one-part geopolymers with different activators. *Construction and Building Materials, 225*, 526–537. https://doi.org/10.1016/J.CONBUILDMAT.2019.07.083

ASTM. (2016). *Standard, c187, standard test method for amount of water required for normal consistency of hydraulic cement paste.* ASTM international west Conshohocken, PA.

ASTM. (2019). *C191-19, standard test methods for time of setting of hydraulic cement by vicat needle.* ASTM International, West Conshohocken, PA. www.astm.org.

ASTM. (2020a). *C109/C109M-20, standard test method for compressive strength of hydraulic cement mortars (using 2-in. or [50 mm] cube specimens).* ASTM international, West Conshohocken, PA. https://doi.org/10.1520/C0109_C0109M-20

ASTM. (2020b). *C1437-20, standard test method for flow of hydraulic cement mortar.* ASTM International, West Conshohocken, PA. www.astm.org, (n.d.). https://doi.org/10.1520/C1437-20

ASTM. (2022). *C989/C989M-22, standard specification for slag cement for use in concrete and mortars.* ASTM International. https://doi.org/10.1520/C0989_C0989M-22

Bishop, M., & Barron, A. R. (2006). Cement hydration inhibition with sucrose, tartaric acid, and lignosulfonate: analytical and spectroscopic study. *Industrial and Engineering Chemistry Research, 45*, 7042–7049. https://doi.org/10.1021/ie060806t

Boström, M., Deniz, V., Franks, G. V., & Ninham, B. W. (2006). Extended DLVO theory: Electrostatic and non-electrostatic forces in oxide suspensions. *Advances in Colloid and Interface Science, 123–126*, 5–15. https://doi.org/10.1016/J.CIS.2006.05.001

Bullard, J. W., Jennings, H. M., Livingston, R. A., Nonat, A., Scherer, G. W., Schweitzer, J. S., Scrivener, K. L., & Thomas, J. J. (2011). Mechanisms of cement hydration. *Cement and Concrete Research, 41*, 1208–1223. https://doi.org/10.1016/J.CEMCONRES.2010.09.011

Collins, F., & Sanjayan, J. G. (1998). Early age strength and workability of slag pastes activated by NaOH and Na$_2$CO$_3$. *Cement and Concrete Research, 28*, 655–664. https://doi.org/10.1016/S0008-8846(98)00025-8

Davidovits, J. (1993). Geopolymer cements to minimize carbon dioxide green-house warming. *Ceramic Transactions, 37*, 165–182.

El Gindy, A. A., Gomaa, E. A., Abdelkader, H. I., Mohsen, A., & Habib, A. O. (2022). The effect of a sulfonated naphthalene-based polymer on redox reaction data, potassium ferrocyanide complexation, and the compressive strength of Portland cement paste. *Journal of Molecular Liquids, 356*, 119000. https://doi.org/10.1016/J.MOLLIQ.2022.119000

El-Feky, M. S., Mohsen, A., El-Tair, A. M., & Kohail, M. (2022). Microstructural investigation for micro–nano-silica engineered magnesium oxychloride cement. *Construction and Building Materials, 342*, 127976. https://doi.org/10.1016/J.CONBUILDMAT.2022.127976

El-Tair, A. M., El-Feky, M. S., Mohsen, A., & Kohail, M. (2021). Properties of nano engineered concrete subjected to accelerated corrosion. *Nanotechnology in Construction, 13*, 1.

Esping, O., & Löfgren, I. (2005). Investigation of early age deformation in self-compacting concrete. In *Knud Hojgaard conference on advanced cement-based materials—research and teaching.*

Essam, Y., El-Faramawy, N., Ramadan, W., & Ramadan, M. (2023). From danger-ous wastes to green construction materials, as thermally stable-radiation blocker, in presence of meso-porous magnesia and alumina. *Journal of Building Engineering, 2023*, 105896.

Feng, D., Provis, J. L., & Van Deventer, J. S. J. (2012). Thermal activation of albite for the synthesis of one-part mix geopolymers. *Journal of the American Ceramic Society, 95*, 565–572. https://doi.org/10.1111/j.1551-2916.2011.04925.x

Folliard, K. J., & Berke, N. S. (1997). Properties of high-performance concrete containing shrinkage-reducing admixture. *Cement and Concrete Research, 27*, 1357–1364. https://doi.org/10.1016/S0008-8846(97)00135-X

Habbaba, A., & Plank, J. (2010). Interaction between polycarboxylate superplas-ticizers and amorphous ground granulated blast furnace slag. *Journal of the American Ceramic Society, 93*, 2857–2863. https://doi.org/10.1111/j.1551-2916.2010.03755.x

Habbaba, A., & Plank, J. (2012). Surface chemistry of ground granulated blast furnace slag in cement pore solution and its impact on the effectiveness

Refaie *et al. Int J Concr Struct Mater*   (2023) 17:48

Page 20 of 22

of polycarboxylate superplasticizers. *Journal of the American Ceramic Society, 95*, 768–775. https://doi.org/10.1111/j.1551-2916.2011.04968.x

Habib, A. O., Aiad, I., El-Hosiny, F. I., & El-Aziz, A. M. A. (2018). Development of the fire resistance and mechanical characteristics of silica fume-blended cement pastes using some chemical admixtures. *Construction and Building Materials, 181*, 163–174. https://doi.org/10.1016/J.CONBUILDMAT.2018.06.051

Habib, A. O., Aiad, I., El-Hosiny, F. I., & Mohsen, A. (2021). Studying the impact of admixtures chemical structure on the rheological properties of silica-fume blended cement pastes using various rheological models. *Ain Shams Engineering Journal, 12*, 1583–1594. https://doi.org/10.1016/J.ASEJ.2020.12.009

Habib, A. O., Aiad, I., Youssef, T. A., & El-Aziz, A. M. A. (2016). Effect of some chemical admixtures on the physico-chemical and rheological properties of oil well cement pastes. *Construction and Building Materials, 120*, 80–88. https://doi.org/10.1016/J.CONBUILDMAT.2016.05.044

Hassan, A., Arif, M., & Shariq, M. (2019). Use of geopolymer concrete for a cleaner and sustainable environment—A review of mechanical properties and microstructure. *Journal of Cleaner Production, 223*, 704–728. https://doi.org/10.1016/j.jclepro.2019.03.051

Hosseini, S., Brake, N. A., Nikookar, M., Günaydın-Şen, Ö., & Snyder, H. A. (2021). Mechanochemically activated bottom ash-fly ash geopolymer. *Cement and Concrete Composites, 118*, 123976. https://doi.org/10.1016/J.CEMCONCOMP.2021.103976

IOP Conference Series: Earth and Environmental Science. (2018). *Optimum mix for fly ash geopolymer binder based on workability and compressive strength, (n.d.)*. https://doi.org/10.1088/1755-1315/140/1/012157

Ismail, I., Bernal, S. A., Provis, J. L., Nicolas, R. S., Hamdan, S., & Van Deventer, J. S. J. (2014). Modification of phase evolution in alkali-activated blast furnace slag by the incorporation of fly ash. *Cement and Concrete Composites, 45*, 125–135. https://doi.org/10.1016/J.CEMCONCOMP.2013.09.006

Jamil, N. H., Abdullah, M. M. A. B., Pa, F. C., Mohamad, H., Ibrahim, W. M. A. W., Amonpattaratkit, P., Gondro, J., Sochacki, W., & Ibrahim, N. (2021). Self-fluxing mechanism in geopolymerization for low-sintering temperature of ceramic. *Materials (basel), 14*, 1–12. https://doi.org/10.3390/ma14061325

Juenger, M. C. G., Winnefeld, F., Provis, J. L., & Ideker, J. H. (2011). Advances in alternative cementitious binders. *Cement and Concrete Research, 41*, 1232–1243. https://doi.org/10.1016/J.CEMCONRES.2010.11.012

Juilland, P., Gallucci, E., Flatt, R., & Scrivener, K. (2010). Dissolution theory applied to the induction period in alite hydration. *Cement and Concrete Research, 40*, 831–844. https://doi.org/10.1016/J.CEMCONRES.2010.01.012

Kashani, A., Provis, J. L., Xu, J., Kilcullen, A. R., Qiao, G. G., & van Deventer, J. S. J. (2014). Effect of molecular architecture of polycarboxylate ethers on plasticizing performance in alkali-activated slag paste. *Journal of Materials Science, 49*, 2761–2772. https://doi.org/10.1007/s10853-013-7979-0

Khaled, Z., Mohsen, A., Soltan, A., & Kohail, M. (2023). Optimization of kaolin into Metakaolin: Calcination Conditions, mix design and curing temperature to develop alkali activated binder. *Ain Shams Engineering Journal, 2023*, 102142.

Labbez, C., Jönsson, B., Pochard, I., Nonat, A., & Cabane, B. (2006). Surface charge density and electrokinetic potential of highly charged minerals: Experiments and Monte Carlo simulations on calcium silicate hydrate. *The Journal of Physical Chemistry B, 110*, 9219–9230.

Lei, L., & Chan, H. K. (2020). Investigation into the molecular design and plasticizing effectiveness of HPEG-based polycarboxylate superplasticizers in alkali-activated slag. *Cement and Concrete Research, 136*, 106150. https://doi.org/10.1016/J.CEMCONRES.2020.106150

Lei, L., & Zhang, Y. (2021). Preparation of isoprenol ether-based polycarboxylate superplasticizers with exceptional dispersing power in alkali-activated slag: Comparison with ordinary Portland cement. *Composites Part B: Engineering, 223*, 109077. https://doi.org/10.1016/J.COMPOSITESB.2021.109077

Li, C., Sun, H., & Li, L. (2010). A review: The comparison between alkali-activated slag (Si + Ca) and metakaolin (Si + Al) cements. *Cement and Concrete Research, 40*, 1341–1349. https://doi.org/10.1016/J.CEMCONRES.2010.03.020

Liu, B., Ke, K., Yang, Y., Miao, D., & He, C. (2022). Preparation and application of low molecular weight polyether polycarboxylate superplasticizer. *Journal of Physics: Conference Series, 2194*, 012035. https://doi.org/10.1088/1742-6596/2194/1/012035

Luukkonen, T., Abdollahnejad, Z., Yliniemi, J., Kinnunen, P., & Illikainen, M. (2018). One-part alkali-activated materials: A review. *Cement and Concrete Research, 103*, 21–34. https://doi.org/10.1016/j.cemconres.2017.10.001

Marchon, D., & Flatt, R. J. (2016a). Mechanisms of cement hydration. *Science and Technology of Concrete Admixtures, 2016*, 129–145. https://doi.org/10.1016/B978-0-08-100693-1.00008-4

Marchon, D., & Flatt, R. J. (2016b). Impact of chemical admixtures on cement hydration. *Science and Technology of Concrete Admixtures, 2016*, 279–304. https://doi.org/10.1016/B978-0-08-100693-1.00012-6

Marchon, D., Mantellato, S., Eberhardt, A. B., Flatt, R. J. (2016a). Adsorption of chemical admixtures. In *Science and technology of concrete admixtures* (pp. 219–256). Elsevier.

Marchon, D., Mantellato, S., Eberhardt, A. B., & Flatt, R. J. (2016b). Adsorption of chemical admixtures. *Science and Technology of Concrete Admixtures, 2016*, 219–256. https://doi.org/10.1016/B978-0-08-100693-1.00010-2

Marchon, D., Sulser, U., Eberhardt, A., & Flatt, R. J. (2013). Molecular design of comb-shaped polycarboxylate dispersants for environmentally friendly concrete. *Soft Matter, 9*, 10719–10728.

Mayhoub, O. A., Mohsen, A., Alharbi, Y. R., Abadel, A. A., Habib, A. O., & Kohail, M. (2021). Effect of curing regimes on chloride binding capacity of geopolymer. *Ain Shams Engineering Journal*. https://doi.org/10.1016/J.ASEJ.2021.04.032

Meletov, K. P. (1991). High pressure study of intermolecular resonance interaction in a naphthalene crystal. *Chemical Physics, 154*, 469–475. https://doi.org/10.1016/0301-0104(91)85029-G

Mohamed, O. A., Hazem, M. M., Mohsen, A., & Ramadan, M. (2023). Impact of microporous γ-Al$_2$O$_3$ on the thermal stability of pre-cast cementitious composite containing glass waste. *Construction and Building Materials, 378*, 131186.

Mohammed, B. S., Haruna, S., Wahab, M. M. A., Liew, M. S., & Haruna, A. (2019). Mechanical and microstructural properties of high calcium fly ash one-part geopolymer cement made with granular activator. *Heliyon., 5*, e02255. https://doi.org/10.1016/J.HELIYON.2019.E02255

Mohsen, A., Abdel-Gawwad, H. A., & Ramadan, M. (2020a). Performance, radiation shielding, and anti-fungal activity of alkali-activated slag individually modified with zinc oxide and zinc ferrite nano-particles. *Construction and Building Materials, 257*, 119584. https://doi.org/10.1016/j.conbuildmat.2020.119584

Mohsen, A., Aiad, I., El-Hossiny, F. I., & Habib, A. O. (2020b). Evaluating the mechanical properties of admixed blended cement pastes and estimating its kinetics of hydration by different techniques. *Egyptian Journal of Petroleum, 29*, 171–186.

Mohsen, A., Amin, M. S., Waly, S. A., & Ramadan, M. (2022a). Rheological behavior, mechanical properties, fire resistance, and gamma ray attenuation capability for eco-friendly cementitious mixes incorporating thermally treated lead sludge. *Construction and Building Materials, 359*, 129479.

Mohsen, A., El-Feky, M. S., El-Tair, A. M., & Kohail, M. (2021). Effect of delayed microwaving on the strength progress of Green alkali activated cement composites. *Journal of Building Engineering, 43*, 103135. https://doi.org/10.1016/J.JOBE.2021.103135

Mohsen, A., Kohail, M., Abadel, A. A., Alharbi, Y. R., Nehdi, M. L., & Ramadan, M. (2022c). Correlation between porous structure analysis, mechanical efficiency and gamma-ray attenuation power for hydrothermally treated slag-glass waste-based geopolymer. *Case Studies in Construction Materials, 17*, 01505. https://doi.org/10.1016/J.CSCM.2022.E01505

Mohsen, A., Ramadan, M., Gharieb, M., Yahya, A., Soltan, A. M., & Hazem, M. M. (2022b). Rheological behaviour, mechanical performance, and anti-fungal activity of OPC-granite waste composite modified with zinc oxide dust. *Journal of Cleaner Production, 341*, 130877. https://doi.org/10.1016/J.JCLEPRO.2022.130877

Möschner, G., Lothenbach, B., Figi, R., & Kretzschmar, R. (2009). Influence of citric acid on the hydration of Portland cement. *Cement and Concrete Research, 39*, 275–282. https://doi.org/10.1016/J.CEMCONRES.2009.01.005

Nasir, M., Johari, M. A. M., Maslehuddin, M., Yusuf, M. O., & Al-Harthi, M. A. (2020). Influence of heat curing period and temperature on the strength of silico-manganese fume-blast furnace slag-based alkali-activated mortar. *Construction and Building Materials, 251*, 118961. https://doi.org/10.1016/j.conbuildmat.2020.118961

Nasr, D., Pakshir, A. H., & Ghayour, H. (2018). The influence of curing conditions and alkaline activator concentration on elevated temperature behavior

of alkali activated slag (AAS) mortars. *Construction and Building Materials, 190*, 108–119. https://doi.org/10.1016/J.CONBUILDMAT.2018.09.099

Nematollahi, B., & Sanjayan, J. (2014). Effect of different superplasticizers and activator combinations on workability and strength of fly ash based geopolymer. *Materials and Design, 57*, 667–672. https://doi.org/10.1016/J.MATDES.2014.01.064

Neupane, K. (2016). Fly ash and GGBFS based powder-activated geopolymer binders: A viable sustainable alternative of Portland cement in concrete industry. *Mechanics of Materials, 103*, 110–122. https://doi.org/10.1016/j.mechmat.2016.09.012

Oderji, S. Y., Chen, B., Ahmad, M. R., & Shah, S. F. A. (2019). Fresh and hardened properties of one-part fly ash-based geopolymer binders cured at room temperature: Effect of slag and alkali activators. *Journal of Cleaner Production, 225*, 1–10. https://doi.org/10.1016/j.jclepro.2019.03.290

Oh, J. E., Monteiro, P. J. M., Jun, S. S., Choi, S., & Clark, S. M. (2010). The evolution of strength and crystalline phases for alkali-activated ground blast furnace slag and fly ash-based geopolymers. *Cement and Concrete Research, 40*, 189–196. https://doi.org/10.1016/J.CEMCONRES.2009.10.010

Ohta, A., Sugiyama, T., & Tanaka, Y. (1997). Fluidizing mechanism and application of polycarboxlate-based superplasticizers. *Special Publications, 173*, 359–378.

Palacios, M., & Puertas, F. (2004). Stability of superplasticizer and shrinkage-reducing admixtures stability of superplasticizer and shrinkage-reducing admixtures in high basic media. *Materiales De Construcción, 54*, 65–86.

Palacios, M., & Puertas, F. (2005). Effect of superplasticizer and shrinkage-reducing admixtures on alkali-activated slag pastes and mortars. *Cement and Concrete Research, 35*, 1358–1367.

Palacios, M., & Puertas, F. (2007). Effect of shrinkage-reducing admixtures on the properties of alkali-activated slag mortars and pastes. *Cement and Concrete Research, 37*, 691–702. https://doi.org/10.1016/j.cemconres.2006.11.021

Palacios, M., Sierra, C., & Puertas, F. (2003). Techniques and methods of characterization of admixtures for the concrete. *Materiales De Construcción, 53*, 89–105.

Plank, J., & Hirsch, C. (2007). Impact of zeta potential of early cement hydration phases on superplasticizer adsorption. *Cement and Concrete Research, 37*, 537–542. https://doi.org/10.1016/J.CEMCONRES.2007.01.007

Puertas, F., Palacios, M., Manzano, H., Dolado, J. S., Rico, A., & Rodríguez, J. (2011). A model for the CASH gel formed in alkali-activated slag cements. *Journal of the European Ceramic Society, 31*, 2043–2056.

Puertas, F., Palomo, A., Fernández-Jiménez, A., Izquierdo, J. D., & Granizo, M. L. (2003). Effect of superplasticisers on the behaviour and properties of alkaline cements. *Advances in Cement Research, 15*, 23–28. https://doi.org/10.1680/adcr.2003.15.1.23

Ramachandran, V. S., Malhotra, V. M., Jolicoeur, C., Spiratos, N. (1998). Superplasticisers: Properties and applications in concrete. *Natural Resources Canada, CANMET*, ISBN: 0-660-17393-X. https://nrc-publications.canada.ca/eng/view/object/?id=ca5965c4-c0bc-478a-a3a5-3bd5ec09186e

Ramadan, M., Amin, M. S., Waly, S. A., & Mohsen, A. (2021). Effect of high gamma radiation dosage and elevated temperature on the mechanical performance of sustainable alkali-activated composite as a cleaner product. *Cement and Concrete Composites, 121*, 104087. https://doi.org/10.1016/J.CEMCONCOMP.2021.104087

Ramadan, M., Habib, A. O., Hazem, M. M., Amin, M. S., & Mohsen, A. (2023a). Synergetic effects of hydrothermal treatment on the behavior of toxic sludge-modified geopolymer: Immobilization of cerium and lead, textural characteristics, and mechanical efficiency. *Construction and Building Materials, 367*, 130249.

Ramadan, M., Kohail, M., Abadel, A. A., Alharbi, Y. R., Tuladhar, R., & Mohsen, A. (2022b). De-aluminated metakaolin-cement composite modified with commercial titania as a new green building material for gamma-ray shielding applications. *Case Studies in Construction Materials, 17*, e01344. https://doi.org/10.1016/j.cscm.2022.e01344

Ramadan, M., Kohail, M., Alharbi, Y. R., Abadel, A. A., Binyahya, A. S., & Mohsen, A. (2023b). Investigation of autoclave curing impact on the mechanical properties, heavy metal stabilization and anti-microbial activity of the green geopolymeric composite based on received/thermally-treated glass polishing sludge. *J. Mater. Res. Technol., 23*, 2672–2689.

Ramadan, M., Ramadan, W., Shwita, F., & El-Faramawy, N. (2022a). Valorization of hazardous glass wastes via geopolymer production utilized in gamma

ray shielding applications: A comparative study with Portland cement. *Radiation Physics and Chemistry, 197*, 110174.

Refaat, M., Mohsen, A., Nasr, E.-S.A.R., & Kohail, M. (2021). Minimizing energy consumption to produce safe one-part alkali-activated materials. *Journal of Cleaner Production, 323*, 129137. https://doi.org/10.1016/J.JCLEPRO.2021.129137

Refaat, M., Mohsen, A., Nasr, E.-S.A.R., & Kohail, M. (2023). Utilization of optimized microwave sintering to produce safe and sustainable one-part alkali-activated materials. *Science and Reports, 13*, 4611.

Refaie, M., Mohsen, A., El-Sayed, A. N., & Kohail, M. (2023). The effect of structural stability of chemical admixtures on the NaOH alkali-activated slag properties. *Journal of Materials in Civil Engineering, 35*, 4022367. https://doi.org/10.1061/(ASCE)MT.1943-5533.0004523

Ren, J. (2016). *Superplasticiser for NaOH-activated slag: Competition and instability between superplasticiser and alkali-activator*.

Sayed, D. G., El-Hosiny, F. I., El-Gamal, S. M. A., Hazem, M. M., & Ramadan, M. (2022). Synergetic impacts of mesoporous α-Fe_2O_3 nanoparticles on the performance of alkali-activated slag against fire, gamma rays, and some microorganisms. *Journal of Building Engineering, 57*, 104947.

Shwita, F., El-Faramawy, N., Ramadan, W., & Ramadan, M. (2021). Investigation of the mechanical properties, morphology and the attenuation behavior of gamma rays for OPC pastes mingled with two different glass wastes. *Construction and Building Materials, 313*, 125475. https://doi.org/10.1016/j.conbuildmat.2021.125475

Soroka, I. (1993). *Concrete in hot environments*. CRC Press.

Tan, J., Cizer, Ö., De Vlieger, J., Dan, H., & Li, J. (2022). Impacts of milling duration on construction and demolition waste (CDW) based precursor and resulting geopolymer: Reactivity, geopolymerization and sustainability. *Resources, Conservation and Recycling, 184*, 106433. https://doi.org/10.1016/J.RESCONREC.2022.106433

Walker, R., & Pavía, S. (2011). Physical properties and reactivity of pozzolans, and their influence on the properties of lime-pozzolan pastes. *Materials and Structures Construction, 44*, 1139–1150. https://doi.org/10.1617/s11527-010-9689-2

Xiong, G., & Guo, X. (2022). Effects and mechanism of superplasticizers and precursor proportions on the fresh properties of fly ash-slag powder based geopolymers. *Construction and Building Materials, 350*, 128734. https://doi.org/10.1016/J.CONBUILDMAT.2022.128734

Yahia, A. (2011). Shear-thickening behavior of high-performance cement grouts—Influencing mix-design parameters. *Cement and Concrete Research, 41*, 230–235. https://doi.org/10.1016/j.cemconres.2010.11.004

Yamada, K., Takahashi, T., Hanehara, S., & Matsuhisa, M. (2000). Effects of the chemical structure on the properties of polycarboxylate-type superplasticizer. *Cement and Concrete Research, 30*, 197–207. https://doi.org/10.1016/S0008-8846(99)00230-6

Yoshioka, K., Sakai, E., Daimon, M., & Kitahara, A. (1997). Role of steric hindrance in the performance of superplasticizers for concrete. *Journal of the American Ceramic Society, 80*, 2667–2671.

Zhang, P., Zheng, Y., Wang, K., & Zhang, J. (2018). A review on properties of fresh and hardened geopolymer mortar. *Composites Part B: Engineering, 152*, 79–95. https://doi.org/10.1016/j.compositesb.2018.06.031

Zingg, A., Winnefeld, F., Holzer, L., Pakusch, J., Becker, S., Figi, R., & Gauckler, L. (2009). Interaction of polycarboxylate-based superplasticizers with cements containing different C3A amounts. *Cement and Concrete Composites, 31*, 153–162. https://doi.org/10.1016/J.CEMCONCOMP.2009.01.005

Zuhua, Z., Xiao, Y., Huajun, Z., & Yue, C. (2009). Role of water in the synthesis of calcined kaolin-based geopolymer. *Applied Clay Science, 43*, 218–223. https://doi.org/10.1016/J.CLAY.2008.09.003

Publisher's Note

Mr. M. Refaie is a Master's student in the Structural Engineering Department at the Faculty of Engineering, Ain Shams University. He specializes in the fields

Refaie *et al. Int J Concr Struct Mater*   (2023) 17:48

Page 22 of 22

concerned with environmental materials, sustainability construction, and energy saving in buildings.

Dr. Alaa Mohsen is an Assistant Professor at Ain Shams University's Faculty of Engineering in the Physics and Mathematics Engineering Department (Chemistry Division). He specializes in the chemistry of building materials (cement and geopolymeric composites), chemical admixtures and waste management. His research interests include improving various properties of building materials, such as mechanical properties, fire resistance, radiation shielding and anti-microbial activity. Much of his work has been centered on mitigating environmental pollution resulting from the building materials industry by achieving sustainability and developing eco-friendly materials based on industrial and agricultural wastes in the manufacturing process.

Prof. Dr. Elsayed Nasr is a Professor at Ain Shams University. He specializes in the areas of building materials. He has authored many publications in highly-ranked journals.

Dr. M. Kohail is an accomplished Associate Professor at Ain Shams University's Faculty of Engineering in the Structural Engineering Department. He specializes in the areas of innovative and eco-friendly building materials, sustainability, and energy in buildings. With extensive research expertise, he has authored several highly regarded publications in leading academic journals. Dr. Kohail has worked with various international research groups across multiple disciplines, providing valuable insights to tackle pressing global challenges. His contributions to the field of sustainable construction and engineering have garnered widespread recognition, establishing him as a prominent thought leader in his area of expertise.